

# Frequency response-based damage identification in frames by minimum constitutive relation error and sparse regularization

Jia Guo<sup>a</sup>, Li Wang<sup>b,\*</sup>, Izuru Takewaki<sup>a</sup>

<sup>a</sup>*Department of architecture and architectural engineering, Kyoto University, Kyoto, Japan*

<sup>b</sup>*Department of applied mechanics and engineering, Sun Yat-sen University, Guangzhou, P.R. China*

---

## Abstract

The objective of this paper is to provide a new damage identification method using frequency response data. In this approach, the inverse identification problem is treated as a nonlinear optimization problem whose objective function is just the constitutive relation error (CRE). To circumvent the ill-posedness of the inverse problem which is caused by use of the possibly insufficient data and enhance the robustness of the identification process, the sparse regularization is introduced where the  $\ell_1$ -norm regularization term is added to the original CRE function. In regard to the minimum solution of the sparse-regularized CRE objective function, the alternating minimization (AM) method is established. The attractive features of the present damage identification approach are: (a) while coping with the sparse regularization, a closed-form solution is obtained due to the decoupling of the CRE function with respect to the damage parameters and hence the sparse regularization term would introduce little computational complexity; (b) the sparse regularization parameters are directly determined by a simple threshold setting method; (c) no sensitivity analysis is involved herein. Numerical examples are conducted to verify the proposed approach and the results show that the sparse regularization obviously improves the accuracy and robustness for the identified damages.

---

\*Corresponding author

*Email address:* wangli75@mail.sysu.edu.cn (Li Wang)

*Keywords:* damage identification, constitutive relation error, sparse regularization, frequency response data, alternating minimization method

---

## 1. Introduction

Academic research regarding vibration-based damage identification has been rapidly expanded over the past decades[1, 2, 3, 4]. The methods, using dynamic response data in the damage identification process, could be classified into two groups: methods based on signals and methods based on models [5]. Signal-based methods received much attention in recent years and have been successfully applied to detect and locate structural damages[6, 7]. They are typically non-parametric methods and able to avoid modeling errors and high computational costs during numerical simulations. However, these methods are hard to assess the damage severity, sensitive to the measurement noise and mostly limited up to small-sized structures[5]. In contrast, the advantage of the methods based on models is obvious: able to identify the damage location and severity simultaneously and capable to take into account all of the available structural information.

Classically, the model-based methods treat damage identification as a constrained nonlinear optimization problem with the structural model parameters such as mass, stiffness and damping forming the basic variables. The objective function of the nonlinear problem is usually set up by measuring the discrepancies between the numerical model and the dynamic test results. The selection of the objective function is a crucial issue. It not only affects the interpretation of the best correlation, but also influences the behavior of the utilized optimization algorithm[8]. Weighted least squares of the errors between the measured data and the derived data is generally chosen as the objective function[9]. To solve this optimization problem, the genetic algorithms (GA) and the sensitivity-based approaches are commonly used[10, 11, 12]. Other optimization methods include the minimization of rank perturbation theory[13] and the 'residual force' method[14].

Recently, usage of the error in constitutive relation has caught the attention of researchers. This idea was first proposed for model updating analysis and then extended to structural damage identification problems in linear statics[15], transient dynamics[16], elastoplastics[17] and so on. In this approach, the objective function is defined as the constitutive relation error (CRE), that is, an energy inner product of the residual of the constitutive equation connecting the admissible stresses and the kinematically admissible displacements. It is remarkable that the CRE objective function is separately convex, which guarantees the appropriate application of the efficient alternating minimization (AM) approach[18, 19], to get the solution of this nonlinear optimization problem. To this end, the sensitivity analysis is no longer needed.

For large scale civil structures, it is often required to identify the structural parameters based on the incomplete structural vibration response measurement data. This is essentially an ill-posed inverse problem which is caused by the possibly insufficient amount of the measurement data. Attempting to circumvent this drawback, regularization techniques such as the Tikhonov regularization and the sparse regularization are always introduced. The idea that all the damages or changes of parameters are as small as possible is implicated in the Tikhonov regularization[20]. Such an idea is reasonable for model updating however, it may not be appropriate for damage identification since large damages may occur. On the other hand, damages always occur at a few locations where maximum-stress/plasticity appears, impact loads work or crack propagates for practical structures. This would be appropriately implicated in the sparse regularization[21, 22], which weakly enforces the sparsity constraint for the damage locations.

In this paper, a new structural damage identification is proposed for the incomplete measured frequency response data using the minimum constitutive relation error (min-CRE) approach and the sparse regularization. The first objective of this paper is to clarify the mathematical advantages of the decoupled CRE objective function with respect to the damage parameters. In fact, the sparse regularization has already been incorporated into the sensitivity-based

approaches[23]. However, it is noteworthy that a linear least-squares function  
60 along with the prescribed sparse regularization is a non-linear and non-quadratic  
function and its minimization shall be obtained through iterative algorithms,  
which is costly compared to the case with the Tikhonov regularization. In  
general, the sparse regularization problem requires significantly greater compu-  
tational effort and no closed-form solution exists. There are several families of  
65 computational methods to get sparse solutions: greedy pursuit, convex relax-  
ation, non-convex optimization, Bayesian framework and brute force[22]. In this  
research, however, the inherent decoupling of the CRE function with respect to  
the damage parameters makes every parameter-update-step solved as a series  
of single-variable optimization problem and hence results in a closed-form so-  
70 lution for the sparse regularization problem. This introduces little additionally  
computational effort caused by the sparse regularization.

The second objective of this paper is to present a novel and simple thresh-  
old setting method to properly determine the sparse regularization parameters.  
There are several ways to obtain the general optimal regularization parame-  
75 ters for inverse problems in mathematics: discrepancy principle (DP)[24], or-  
dinary and generalized cross validations (GCV)[25], L-curve criterion[26] and  
so on. However, the selection criterion for the sparse regularization is very  
limited because the problem generally has no closed-form solution. An appro-  
priate regularization parameter is typically selected by experience[27, 28]. The  
80 reference[29] proposed two possible strategies of selecting the sparse regular-  
ization parameter: the first selection method utilizes the residual and solution  
norms to determine the appropriate range of the regularization parameter while  
the other is developed based on the DP. In both strategies, the linear least-  
squares problems under several trial sparse regularization parameters should be  
85 solved and this obviously leads to prohibitively high computation cost. In this  
paper, the determination of the regularization parameter would be straightfor-  
ward and require no repeated computation by the proposed threshold setting  
method.

In this research, the frequency response function (FRF) and natural frequen-

90 cies data, directly extracted from the dynamic test, are used as the measured  
 data. Vibration-based damage identification using FRF measurements has been  
 studied by a number of references[30, 31] and it has been proved that FRF data  
 are more reliable and practical to provide abundant information at measured  
 degrees of freedom and at a great number of desired frequencies[32] without  
 95 being contaminated by any modal extraction errors and loss of information.  
 Particular attention should be paid to properly select the frequency ranges of  
 the FRF data. The remainder of this paper is organized as follows. The basic  
 inverse identification problem by the min-CRE principle is introduced in Sec-  
 tion 2. In Section 3, the sparse regularization is applied to enhance the CRE  
 100 objective function and then, an AM method is applied to solve this nonlinear  
 optimization problem. Numerical tests are performed in Section 4 and final  
 conclusions are drawn in Section 5.

## 2. Problem statement

### 2.1. The baseline model

105 Consider an elastic structure occupying the open domain  $\Omega$  and bounded  
 by the boundary  $\partial\Omega$ . The vibration of this linear elastic problem in frequency  
 domain is divided into three sets of differential equations for the displacement  
 field  $\mathbf{u}$  and the stress field  $\boldsymbol{\sigma}$ .

- **Kinematic constraints**

$$\mathbf{u} \in \mathcal{U} := \begin{cases} \boldsymbol{\varepsilon} = \boldsymbol{\mathcal{S}}\mathbf{u} & \text{in } \Omega \\ \mathbf{u} = \mathbf{u}_p & \text{over } \partial\Omega_u \end{cases} \quad (1)$$

110 where  $\boldsymbol{\mathcal{S}}$  is a suitable linear differential operator and  $\mathbf{u}_p$  is the prescribed  
 value of the displacement field  $\mathbf{u}$  on the Dirichlet boundary  $\partial\Omega_u$ .  $\boldsymbol{\varepsilon}$  rep-  
 represents the deformation tensor.

- **Equilibrium equations**

$$\boldsymbol{\sigma} \in \mathfrak{S} := \begin{cases} \boldsymbol{\mathcal{L}}\boldsymbol{\sigma} + \mathbf{b} = \boldsymbol{\tau} & \text{in } \Omega \\ \boldsymbol{\sigma} \cdot \mathbf{n} = \mathbf{t} & \text{over } \partial\Omega_f \end{cases} \quad (2)$$

where  $\mathcal{L}$  is the divergence operator on stress field  $\boldsymbol{\sigma}$  and  $n$  the external unit vector normal to the Neumann boundary  $\partial\Omega_f$ . Over  $\partial\Omega_f$ , the traction field  $\mathbf{t}$  is prescribed. In addition,  $\mathbf{b}$  denotes the body force while  $\boldsymbol{\tau}$  the inertial force.

• **Constitutive relations**

$$\begin{cases} \boldsymbol{\sigma} = \mathbb{D} : \boldsymbol{\varepsilon} \text{—Hooke's law,} \\ \boldsymbol{\tau} = -\omega^2 \rho \mathbf{u} \text{—Newton's law.} \end{cases} \quad (3)$$

where  $\mathbb{D} \in \mathcal{C}$  is an elastic modulus tensor with appropriate material properties and  $\rho$  is the density which is assumed to be constant in this research. It should be noted that only the case of forced vibrations problems are considered and the equations are written in the frequency domain with  $\omega$  being the angular frequency herein.

2.2. *CRE function for a given frequency*

To define the constitutive relation error (CRE), consider an admissible pair  $(\mathbf{u}, \boldsymbol{\sigma})$  which satisfies the kinematic constraints (equation (1)) and the equilibrium equations (equation (2)) respectively. It is easily known that, if the constitutive relations (equation (3)) are additionally satisfied with an admissible elastic modulus tensor  $\mathbb{D}$ , the above admissible solution trio  $(\mathbf{u}, \boldsymbol{\sigma}, \mathbb{D})$  would be the exact solution  $(\mathbf{u}_{\text{ex}}, \boldsymbol{\sigma}_{\text{ex}}, \mathbb{D}_{\text{ex}})$  of this dynamic linear elastic problem.

As a result, to measure the distance from the admissible solution to the exact solution in the energy product, the CRE for a given frequency is expressed as

$$e_{CRE}(\mathbf{u}, \boldsymbol{\sigma}, \mathbb{D}) = \frac{1}{2} \int_{\Omega} \left\{ r_1 \text{Tr} [(\boldsymbol{\sigma} - \mathbb{D} : \boldsymbol{\varepsilon}(\mathbf{u})) : \mathbb{D}^{-1} : (\boldsymbol{\sigma} - \mathbb{D} : \boldsymbol{\varepsilon}(\mathbf{u}))] + r_2 (\rho\omega^2)^{-1} [(\boldsymbol{\tau}(\boldsymbol{\sigma}) + \rho\omega^2 \mathbf{u}) : (\boldsymbol{\tau}(\boldsymbol{\sigma}) + \rho\omega^2 \mathbf{u})] \right\} d\Omega \quad (4)$$

where  $r_1, r_2$  are the corresponding weight coefficients ( $r_1 + r_2 = 1$ ). The values of these coefficients depend on the relative reliability between the constitutive relations based on the Hooke's law and based on the Newton's law and are fixed to be  $r_1 = r_2 = 0.5$  in this work.

Further considering the kinematic constrains and the equilibrium equations, the CRE in equation (4) could be rewritten as

$$e_{CRE}(\mathbf{u}, \boldsymbol{\sigma}, \mathbb{D}) = \frac{1}{2} \int_{\Omega} \left\{ r_1 \text{Tr} [(\boldsymbol{\sigma} - \mathbb{D} : \boldsymbol{S}\mathbf{u}) : \mathbb{D}^{-1} : (\boldsymbol{\sigma} - \mathbb{D} : \boldsymbol{S}\mathbf{u})] + r_2 (\rho\omega^2)^{-1} [(\mathcal{L}\boldsymbol{\sigma} + \mathbf{b} + \rho\omega^2\mathbf{u}) : (\mathcal{L}\boldsymbol{\sigma} + \mathbf{b} + \rho\omega^2\mathbf{u})] \right\} d\Omega \quad (5)$$

For the structure which is of interest in a frequency range  $[\omega_{\min}, \omega_{\max}]$ , the frequency weighting factor  $z(\omega)$  is introduced

$$\int_{\omega_{\min}}^{\omega_{\max}} z(\omega) = 1, \quad z(\omega) > 0 \quad (6)$$

Then the total CRE in the given frequency range is established as

$$F(\mathbf{u}, \boldsymbol{\sigma}, \mathbb{D}) := \int_{\omega_{\min}}^{\omega_{\max}} e_{CRE}(\mathbf{u}, \boldsymbol{\sigma}, \mathbb{D}) z(\omega) d\omega \quad (7)$$

Based on the equations above, the damage identification problem is formulated as

$$\begin{aligned} & \arg \min F(\mathbf{u}, \boldsymbol{\sigma}, \mathbb{D}) \\ & \text{subject to } \mathbf{u} \in \mathcal{U}, \boldsymbol{\sigma} \in \mathfrak{S}, \mathbb{D} \in \mathcal{C}, \mathbf{u} = \hat{\mathbf{u}}_k, k \in \wp \end{aligned} \quad (8)$$

where  $\{\hat{\mathbf{u}}_k, k \in \wp\}$  is the incomplete frequency response data measured by finite sensors on the set of points  $\{k \in \wp\}$ . Equation (8) is known as the min-CRE principle for inverse identification problems [33, 34] and  $F(\mathbf{u}, \boldsymbol{\sigma}, \mathbb{D})$  is known as the CRE objective function. For each frequency  $\omega_i$ ,  $z(\omega_i)$  is taken equally herein. The CRE function is chosen as the objective function in this research due to the following crucial features,

- Separate convexity: the separately convex property of the proposed objective function is of critical importance for the application of the alternating minimization(AM) method because only then, each alternating step become well-posed[35]. (Refer to section 3.1)
- Decoupling with respect to the damage parameters: under the constant stiffness assumption in every element, the CRE objective function is decoupled with respect to the damage parameters, or specifically, minimization

145 of the CRE objective function over the damage parameters gives rise to a series of single-variable minimization problems. With the decoupled objective function, the sparse regularization, which is to be introduced later, will be easily tackled by the closed-form solution with little additional computational efforts. (Refer to section 3.3)

150 *2.3. Discrete formulation of the CRE function*

In the following, the inverse identification problem is solved in a finite element environment which requires to discretize the CRE objective function at first. A typical finite element,  $e$ , is defined by local nodes  $i, j, k, \dots$  and for each frequency, the displacement  $\mathbf{u}$  and stress  $\boldsymbol{\sigma}$  and the trial counterparts  $\delta\mathbf{u}$  and  $\delta\boldsymbol{\sigma}$  within the element  $e$  is approximated as

$$\begin{cases} \mathbf{u} \approx \mathbf{N}_1 \tilde{\mathbf{u}}^e, \delta\mathbf{u} \approx \mathbf{N}_1 \delta\tilde{\mathbf{u}}^e \\ \boldsymbol{\sigma} \approx \mathbf{N}_2 \tilde{\mathbf{q}}^e = \mathbf{N}_2 \tilde{\mathbf{q}}_0^e + \mathbf{N}_2 \tilde{\mathbf{q}}_p^e, \delta\boldsymbol{\sigma} \approx \mathbf{N}_2 \delta\tilde{\mathbf{q}}^e = \mathbf{N}_2 \delta\tilde{\mathbf{q}}_0^e \end{cases} \quad (9)$$

where  $\mathbf{N}_1$  and  $\mathbf{N}_2$  are called shape functions (or interpolation functions) corresponding to nodal displacement vector  $\tilde{\mathbf{u}}^e$  and nodal force vector  $\tilde{\mathbf{q}}^e$  separately. The nodal force  $\tilde{\mathbf{q}}^e$ , obtained from a mathematical integration of stress  $\boldsymbol{\sigma}$ , is dynamically equivalent to the addition of the boundary forces  $\tilde{\mathbf{q}}_p^e$  and the remaining  
 155 homogeneous forces  $\tilde{\mathbf{q}}_0^e$ . As is noteworthy, the inhomogeneous part  $\mathbf{N}_2^T \tilde{\mathbf{q}}_p^e$  vanish in the virtual stress  $\delta\boldsymbol{\sigma}$ . Additionally, the nodal force  $\tilde{\mathbf{q}}^e$  should contain the same number of components as the corresponding nodal displacement  $\tilde{\mathbf{u}}^e$  and be ordered in the appropriate corresponding directions. For three-dimensional beam elements, details on the expressions for the nodal displacement vector  $\tilde{\mathbf{u}}^e$   
 160 and the nodal force vector  $\tilde{\mathbf{q}}^e$  and the derivation for the shape functions  $\mathbf{N}_1$  and  $\mathbf{N}_2$  are given in Appendix.

Using equations (1) and (2), one could also obtain the following expression.

$$\begin{cases} \boldsymbol{\varepsilon} = \mathcal{S}\mathbf{u} \approx \mathcal{S}\mathbf{N}_1 \tilde{\mathbf{u}}^e = \mathbf{B}_1 \tilde{\mathbf{u}}^e \\ \mathcal{L}\boldsymbol{\sigma} \approx \mathcal{L}\mathbf{N}_2 \tilde{\mathbf{q}}^e = \mathbf{B}_2 \tilde{\mathbf{q}}^e \end{cases} \quad (10)$$

With these preparations and further considering the CRE in equation (5), one

can have the discrete form of the CRE as follows.

$$e_{CRE}(\tilde{\mathbf{u}}, \tilde{\mathbf{q}}, \mathbf{D}) = \frac{1}{2} \int_{\Omega} \left\{ r_1 (\mathbf{N}_2 \tilde{\mathbf{q}} - \mathbf{D} \mathbf{B}_1 \tilde{\mathbf{u}})^T \mathbf{D}^{-1} (\mathbf{N}_2 \tilde{\mathbf{q}} - \mathbf{D} \mathbf{B}_1 \tilde{\mathbf{u}}) + r_2 (\rho \omega^2)^{-1} (\mathbf{B}_2 \tilde{\mathbf{q}} + \mathbf{b} + \rho \omega^2 \mathbf{N}_1 \tilde{\mathbf{u}})^T (\mathbf{B}_2 \tilde{\mathbf{q}} + \mathbf{b} + \rho \omega^2 \mathbf{N}_1 \tilde{\mathbf{u}}) \right\} d\Omega \quad (11)$$

As for damage identification, the damage parameters  $\tilde{\boldsymbol{\theta}} = [\theta_0 := 1; \theta_1; \dots; \theta_N]$ ,  $0 \leq \theta_e \leq 1$ ,  $e = 1, 2, \dots, N$  with  $\theta_e = 1$  meaning no damage of the  $e$ th element are assumed to be linearly implicated in the elastic matrix  $\mathbf{D}$ , or in other words, the elastic matrix  $\mathbf{D}$  is an affine function of the damage parameters  $\boldsymbol{\theta}$ , i.e.,  $\mathbf{D} = \mathbf{D}(\tilde{\boldsymbol{\theta}}) := \theta_e \mathbf{D}_e$  for element  $e$  where  $\mathbf{D}_e$  is termed the elemental elastic matrix of the intact structure. Obviously, for an intact structure, there is  $\tilde{\boldsymbol{\theta}} = \tilde{\boldsymbol{\theta}}_0 := [1; 1; \dots; 1]$ . As a result, equation(11) can be equally described as

$$e_{CRE}(\tilde{\mathbf{u}}, \tilde{\mathbf{q}}, \tilde{\boldsymbol{\theta}}) = \frac{1}{2} \sum_{e=1}^N \int_{\Omega^e} \left\{ r_1 (\mathbf{N}_2 \tilde{\mathbf{q}}^e - \theta_e \mathbf{D}_e \mathbf{B}_1 \tilde{\mathbf{u}}^e)^T (\theta_e \mathbf{D}_e)^{-1} (\mathbf{N}_2 \tilde{\mathbf{q}}^e - \theta_e \mathbf{D}_e \mathbf{B}_1 \tilde{\mathbf{u}}^e) + r_2 (\rho \omega^2)^{-1} (\mathbf{B}_2 \tilde{\mathbf{q}}^e + \mathbf{b} + \rho \omega^2 \mathbf{N}_1 \tilde{\mathbf{u}}^e)^T (\mathbf{B}_2 \tilde{\mathbf{q}}^e + \mathbf{b} + \rho \omega^2 \mathbf{N}_1 \tilde{\mathbf{u}}^e) \right\} d\Omega \quad (12)$$

With these notification, it is obvious that the CRE objective function (12) is decoupled with respect to the damage parameters  $\tilde{\boldsymbol{\theta}}$ , i.e., in every single equation of the equation (12), only one of the parameters  $\tilde{\boldsymbol{\theta}}$  arises. Such a decoupling will act as a particular role in later analysis when the sparse regularization is considered.

#### 2.4. Sparse regularization

In practice, the amount of the measured data is always limited and this may make the damage identification problem ill-posed and very sensitive to the measurement noise. To circumvent the ill-posedness and improve the robustness, the sparse regularization technique is reasonably introduced. The main prerequisite is that the change of damage parameters  $\tilde{\boldsymbol{\theta}} - \tilde{\boldsymbol{\theta}}_0$  must be sparse and no other information regarding the damage is required. By incorporating the sparse regularization into the objective function, the damage identification

problem is reformulated as

$$\begin{aligned}
e_{CRE}(\tilde{\mathbf{u}}, \tilde{\mathbf{q}}, \tilde{\boldsymbol{\theta}}) = & \frac{1}{2} \int_{\Omega} \left\{ r_1 (\mathbf{N}_2 \tilde{\mathbf{q}} - \mathbf{D}(\tilde{\boldsymbol{\theta}}) \mathbf{B}_1 \tilde{\mathbf{u}})^T \mathbf{D}(\tilde{\boldsymbol{\theta}})^{-1} (\mathbf{N}_2 \tilde{\mathbf{q}} - \mathbf{D}(\tilde{\boldsymbol{\theta}}) \mathbf{B}_1 \tilde{\mathbf{u}}) + \right. \\
& r_2 (\rho \omega^2)^{-1} (\mathbf{B}_2 \tilde{\mathbf{q}} + \mathbf{b} + \rho \omega^2 \mathbf{N}_1 \tilde{\mathbf{u}})^T (\mathbf{B}_2 \tilde{\mathbf{q}} + \mathbf{b} + \rho \omega^2 \mathbf{N}_1 \tilde{\mathbf{u}}) \left. \right\} d\Omega \\
& \lambda \|\boldsymbol{\Delta}(\tilde{\boldsymbol{\theta}} - \tilde{\boldsymbol{\theta}}_0)\|_1^1
\end{aligned} \tag{13}$$

where  $\boldsymbol{\Delta} = \text{diag}([\Delta_1, \dots, \Delta_N])$  is the diagonal matrix of elemental length/area/volume for beam/plate/solid element respectively. The  $\ell_1$ -norm  $\|\mathbf{x}\|_1 = \sum_{e=1}^N |x_e|$  defines the sparse regularization term and  $\lambda > 0$  is the corresponding regularization parameter which controls the trade-off between the sparsity and the residual norm. It has been proved that minimization of  $\ell_1$ -norm could satisfy the desired sparsity requirement[36]. Moreover,  $\|\mathbf{x}\|_1$  is still convex and the linear programming techniques[36] can be easily called to solve the optimization problem in the conventional linear least squares setting. In the next section, the AM method is called to get the solution of the sparse-regularized CRE objective function (13). To get a better perspective of the sparsity-promoting nature of  $\ell_1$ -norm regularization, consider a simple structural system (see **Figure 1**) with displacement degree of freedoms  $x$  and the potential energy of the system is designated as  $f(x)$ . If all masses are placed on a frictional surface with the same threshold value of the static friction force  $\lambda$  (see **Figure 1(b)**), the potential energy would be changed into  $f_\lambda(x) = f(x) + \lambda\|x\|_1^1$ , which is equivalent to the  $\ell_1$ -norm regularization. As is noteworthy, if the prescribed friction  $\lambda$  is greater than the maximum of the forces exerted on all masses, no movement  $x = 0$  would occur, while if the prescribed friction  $\lambda$  is less than the  $k(\ll m)$  greatest ones of the forces exerted on all masses but larger than others,  $k$  masses corresponding to  $k$  greatest forces would admit some movement and others keep unmoved; this leads to the sparse solution of  $x$ . To conclude, with a proper choice of  $\lambda$ , the sparsity of the solution  $x$  can be reached by the  $\ell_1$ -norm regularization and therefore, the  $\ell_1$ -norm term  $\lambda\|x\|_1^1$  can indeed serve for the sparse regularization.

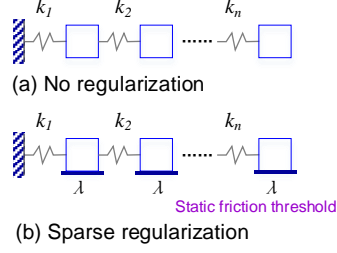


**Figure 1** Physical interpretation of sparse regularizations

### 3. Alternating minimization method for damage identification

#### 3.1. The AM method

In this section, the AM method is proposed to practically solve this nonlinear optimization problem (13). It is shown that the AM method could lower the computational costs associated to the minimization of the CRE objective function than the traditional direct way[19]. Actually, the AM method has been a suitable approach for minimum solution of the separately convex objective function and in principle, it tries to get the solution iteratively by alternating minimization of the objective function over every separated variable in each iteration. Specifically, given the initial damage parameters  $\tilde{\theta}_0$  as those of the intact structure, the solution is obtained successively for  $n = 1, 2, \dots$  as follows

- step 1 (UMF step): Update the mechanical field  $(\tilde{\mathbf{u}}, \tilde{\mathbf{q}})$  with the given damage parameters  $\tilde{\theta}^n$  for each given frequency

$$(\tilde{\mathbf{u}}^{n+1}, \tilde{\mathbf{q}}^{n+1}) = \arg \min_{u \in \mathcal{U}, \sigma \in \mathfrak{S}, u = \hat{u}_k, k \in \wp} F(\tilde{\mathbf{u}}, \tilde{\mathbf{q}}, \tilde{\theta}^n) \quad (14)$$

- step 2 (UDP step): Update the damage parameters  $\tilde{\theta}$  by the mechanical fields  $(\tilde{\mathbf{u}}^{n+1}, \tilde{\mathbf{q}}^{n+1})$  obtained in step 1.

$$\tilde{\theta}^{n+1} = \arg \min_{\tilde{\theta}} F(\tilde{\mathbf{u}}^{n+1}, \tilde{\mathbf{q}}^{n+1}, \tilde{\theta}) \quad (15)$$

#### 3.2. The UMF Step

The mechanical field  $(\tilde{\mathbf{u}}, \tilde{\mathbf{q}})$  is recovered from the measured data and the given damage parameters  $\tilde{\theta}$  (given elastic matrix  $\mathbf{D}$ ) individually for each given

frequency. The sparse regularization term is not involved in this step. Specifically, the minimization over  $\tilde{\mathbf{q}}$  yields the equation:

$$\int_{\Omega} \{r_1 (\mathbf{N}_2^T \mathbf{D}^{-1} \mathbf{N}_2 \tilde{\mathbf{q}} - \mathbf{N}_2^T \mathbf{B}_1 \tilde{\mathbf{u}}) + r_2 ((\rho\omega^2)^{-1} \mathbf{B}_2^T \mathbf{B}_2 \tilde{\mathbf{q}} + \mathbf{B}_2^T \mathbf{N}_1 \tilde{\mathbf{u}} + (\rho\omega^2)^{-1} \mathbf{B}_2^T \mathbf{b})\} = 0 \quad (16)$$

and the minimization over  $\tilde{\mathbf{u}}$  yields

$$\int_{\Omega} \{r_1 (\mathbf{B}_1^T \mathbf{D} \mathbf{B}_1 \tilde{\mathbf{u}} - \mathbf{B}_1^T \mathbf{N}_2 \tilde{\mathbf{q}}) + r_2 (\rho\omega^2 \mathbf{N}_1^T \mathbf{N}_1 \tilde{\mathbf{u}} + \mathbf{N}_1^T \mathbf{B}_2 \tilde{\mathbf{q}} + \mathbf{N}_1^T \mathbf{b})\} = 0 \quad (17)$$

From equations (16) and (17), the mechanical field  $(\tilde{\mathbf{u}}, \tilde{\mathbf{q}})$  can be updated simultaneously. Moreover, equation (17) could be simplified as

$$\begin{pmatrix} (r_1 \mathbf{C}_0 + \frac{r_2}{\omega^2} \mathbf{H}_0) & \mathbf{A}_0 \\ \mathbf{A}_0^T & (r_1 \mathbf{K}_0 + r_2 \omega^2 \mathbf{M}_0) \end{pmatrix} \begin{pmatrix} \tilde{\mathbf{q}} \\ \tilde{\mathbf{u}} \end{pmatrix} = \begin{pmatrix} \mathbf{d}_1 \\ \mathbf{d}_2 \end{pmatrix} \quad (18)$$

where

$$\begin{aligned} \mathbf{C} &= \int_{\Omega} \mathbf{N}_2^T \mathbf{D}^{-1} \mathbf{N}_2 d\Omega, \\ \mathbf{H} &= \int_{\Omega} \frac{1}{\rho} \mathbf{B}_2^T \mathbf{B}_2 d\Omega, \\ \mathbf{M} &= \int_{\Omega} \rho \mathbf{N}_1^T \mathbf{N}_1 d\Omega, \\ \mathbf{K} &= \int_{\Omega} \mathbf{B}_1^T \mathbf{D} \mathbf{B}_1 d\Omega, \\ \mathbf{A} &= \int_{\Omega} (-r_1 \mathbf{N}_2^T \mathbf{B}_1 + r_2 \mathbf{B}_2^T \mathbf{N}_1) d\Omega, \\ \mathbf{d}_1 &= \int_{\Omega} \{-r_2 (\rho\omega^2)^{-1} \mathbf{B}_2^T \mathbf{b} - (r_1 \mathbf{N}_2^T \mathbf{D}^{-1} \mathbf{N}_2 + r_2 (\rho\omega^2)^{-1} \mathbf{B}_2^T \mathbf{B}_2) \tilde{\mathbf{q}}_p\} d\Omega, \\ \mathbf{d}_2 &= \int_{\Omega} \{-r_2 \mathbf{N}_1^T \mathbf{b} - (-r_1 \mathbf{B}_1^T \mathbf{N}_2 + r_2 \mathbf{N}_1^T \mathbf{B}_2) \tilde{\mathbf{q}}_p\} d\Omega. \end{aligned} \quad (19)$$

In equation (19),  $\mathbf{A}_0$ ,  $\mathbf{C}_0$ ,  $\mathbf{K}_0$ ,  $\mathbf{M}_0$  and  $\mathbf{H}_0$  are the reduced forms of  $\mathbf{A}$ ,  $\mathbf{C}$ ,  $\mathbf{K}$ ,  $\mathbf{M}$  and  $\mathbf{H}$  after applying the homogeneous boundary conditions.

To enforce the incomplete measured data, the displacements vector  $\tilde{\mathbf{u}}$  will now be partitioned symbolically into unmeasured displacement  $\tilde{\mathbf{u}}^U$  and measured displacement  $\hat{\mathbf{u}}^M$ . For the sake of convenience, in the following equations

superscript  $U$  and  $M$  represent the corresponding unmeasured and measured DOFs of the array respectively. As a result, equation (18) can be rewritten as

$$\mathbf{L}(\tilde{\boldsymbol{\theta}}) (\tilde{\mathbf{q}}, \tilde{\mathbf{u}}^U)^T = \mathbf{S}(\tilde{\boldsymbol{\theta}}) \quad (20)$$

where

$$\begin{aligned} \mathbf{L}(\tilde{\boldsymbol{\theta}}) &= \begin{pmatrix} r_1 \mathbf{C}_0 + \frac{r_2}{\omega^2} \mathbf{H}_0 & \mathbf{A}_0 \\ \mathbf{A}_0^T & (r_1 \mathbf{K}_0 + r_2 \omega^2 \mathbf{M}_0)^{UU} \end{pmatrix}, \\ \mathbf{S}(\tilde{\boldsymbol{\theta}}) &= (\mathbf{d}_1, (\mathbf{d}_2^U)_n)^T, \\ \mathbf{d}_2^U &= \mathbf{d}_2^U - (r_1 \mathbf{K}_0 + r_2 \omega^2 \mathbf{M}_0)^{UM} \hat{\mathbf{u}}^M \end{aligned} \quad (21)$$

### 3.3. The UDP Step

Due to the decoupling of the CRE objective function (7) as mentioned in Section 2.4, the UDP step is tackled by solving a series of single-variable optimization problems, that is, minimization of equation (13) with respect to  $\theta_e$  for each element  $e$  ( $e = 1, 2, \dots, N$ ) takes the form

$$\begin{aligned} \int_{\Omega^e} \frac{r_1}{2} \left\{ (\mathbf{N}_2 \tilde{\mathbf{q}}^e)^T \frac{(\mathbf{D}_e)^{-1}}{(\theta_e)^2} (\mathbf{N}_2 \tilde{\mathbf{q}}^e) - (\mathbf{B}_1 \tilde{\mathbf{u}}^e)^T \mathbf{D}_e (\mathbf{B}_1 \tilde{\mathbf{u}}^e) \right\} dx \\ - \lambda \Delta^e \{\text{sign}(\theta_e - 1)\} dx = 0. \end{aligned} \quad (22)$$

Finally, one has

$$\theta_e = \begin{cases} \sqrt{\frac{b_e}{a_e + \lambda \Delta^e}}, & \text{if } \lambda < \Lambda_e \\ \sqrt{\frac{b_e}{a_e - \lambda \Delta^e}}, & \text{if } \lambda < -\Lambda_e \\ 1, & \text{if } \lambda \geq |\Lambda_e| \end{cases}, \quad e = 1, 2, \dots, N \quad (23)$$

where

$$\begin{aligned} \Lambda_e &= \frac{1}{\Delta^e} \int_{\Omega_e} \frac{r_1}{2} \left\{ (\mathbf{N}_2 \tilde{\mathbf{q}}^e)^T (\mathbf{D}_e)^{-1} (\mathbf{N}_2 \tilde{\mathbf{q}}^e) - (\mathbf{B}_1 \tilde{\mathbf{u}}^e)^T \mathbf{D}_e (\mathbf{B}_1 \tilde{\mathbf{u}}^e) \right\} d\Omega \\ &= \frac{1}{\Delta^e} (b_e - a_e) \end{aligned} \quad (24)$$

and

$$a_e = \int_{\Omega_e} \frac{r_1}{2} (\mathbf{B}_1 \tilde{\mathbf{u}}^e)^T \mathbf{D}_e (\mathbf{B}_1 \tilde{\mathbf{u}}^e) d\Omega, \quad b_e = \int_{\Omega_e} \frac{r_1}{2} (\mathbf{N}_2 \tilde{\mathbf{q}}^e)^T (\mathbf{D}_e)^{-1} (\mathbf{N}_2 \tilde{\mathbf{q}}^e) d\Omega \quad (25)$$

Detailed explanations of  $\Lambda_e$  are discussed in the next section. Based on equation (23), the value of  $\theta_e$  is found to be prone to be unchanged from the initial value 1 when  $|\Lambda_e| \leq \lambda$  while  $\theta_e$  begin to deviate from 1 to  $\hat{\theta}_e$  when  $|\Lambda_e| \geq \lambda$ . That is to say, the regularization parameter  $\lambda$  determines whether damage occurs: as long as  $\lambda < |\Lambda_e|$ , the  $e$ th element would admit stiffness change or damage; otherwise if  $\lambda \geq |\Lambda_e|$ , the damage would be found to not occur in the  $e$ th element.

Moreover, from equations (22) and (23), the sparse regularization term would introduce little computational complexity and the minimization over each damage parameter along with the sparse regularization term is solved immediately by the closed-form solution in equation (23). This advantage is benefit from the decoupling of the CRE objective function with respect to the damage parameters.

#### 3.4. Regularization Parameter Estimation

As shown in many references[37, 38], the regularization parameter  $\lambda$  plays an important role in the quality of the damage identification results, especially in cases where high levels of noise are present in the data. In this section, a novel and simple strategy, named 'threshold setting method', for estimating the optimal regularization parameter  $\lambda_{\text{est}}$ , is devised.

For each iterative step,  $\mathbf{\Lambda} = \{|\Lambda_e|, e = 1, 2, \dots, N\}$  could be obtained for each element by equation (24). In fact,  $\lambda$  is used to distinguish the damaged elements from the undamaged elements and  $|\Lambda_e|$  reflects the difference between the stiffness parameter obtained directly from the CRE objective function without sparsity ( $\hat{\theta}_e$ ) and the undamaged stiffness parameter ( $\theta_e = 1$ ) for each element. It is easily known that if this difference is large enough ( $|\Lambda_e| > \lambda$ ), damage is reasonably assumed to occur. In other words, elements with higher values of  $|\Lambda_e|$  are likely to be damaged with stronger possibility while lower values indicate undamage and perturbation errors. Thus, setting one of the values in  $\mathbf{\Lambda}$  as threshold could separate the damaged and undamaged elements.

As a result, a simple procedure called 'the threshold setting method' to estimate the optimal regularization parameter  $\lambda_{\text{est}} = \text{TSM}(\mathbf{\Lambda}, l_{\text{max}}, \alpha)$  is proposed

for each iterative step as follows:

1. Get  $\mathbf{\Lambda} = \{|\Lambda_e|, e = 1, 2, \dots, N\}$  from equation (24) and sort the absolute values in the descending order, leading to  $\{\hat{\Lambda}_1 \geq \hat{\Lambda}_2 \geq \dots\}$ ;
- 240 2. Fix the maximum threshold setting rank  $l_{\max}$  and the discriminating ratio  $\alpha$ ;
3. Obtain the optimal regularization parameter  $\lambda_{\text{est}}$ : for each  $l = 1, \dots, l_{\max} - 1$ ,

$$\lambda_{\text{est}} = \begin{cases} \hat{\Lambda}_{l+1}, & \text{if } \hat{\Lambda}_l \geq \alpha \cdot \hat{\Lambda}_{l+1} \\ \hat{\Lambda}_{l_{\max}}, & \text{else} \end{cases} \quad (26)$$

The maximum threshold setting rank  $l_{\max}$  limits the maximum number of possible damages and principally one tends to choose a relatively small value of  $l_{\max}$  to guarantee the sparsity of the identification results. On the other hand, it is conceivable that the general undamaged elements have relatively small values of  $|\Lambda_e|$  corresponding to the noise level and would be quite away from  $|\Lambda_e|$  of the damaged elements. As a result, the discrimination ratio  $\alpha$  measures the distance between the minimum error caused by possible damages and the maximum error purely invoked by the measurement noise level. If  $\hat{\Lambda}_l$  is much greater than  $\hat{\Lambda}_{l+1}$  ( $\hat{\Lambda}_l \geq \alpha \cdot \hat{\Lambda}_{l+1}$ ), element  $l$  is identified as damaged. The maximum threshold setting rank  $l_{\max}$  gives possible maximum number (initial guess) of damages while the discrimination ratio  $\alpha$  narrow it down. More discussions on the choice of  $(l_{\max}, \alpha)$  could be found in Section 4.1.

### 255 3.5. Summary of the AM method

By combining the UMF step in Section 3.2 and the UDP step in Section 3.3, using the proposed threshold setting method so as to estimate the optimal regularization parameter  $\lambda$  in Section 3.4, the damage identification algorithm by min-CRE and sparse regularization can be established as shown in **Table 1**. It should be noted that different analysis models could be applied in the UMF step and the UDP step. In the UMF step, more elements are recommended so

as to avoid the discretization error for the mechanical field analysis, while less elements could be used in the UDP step to mitigate the ill-posed problem if acquiring less damage parameters. Nevertheless, as the sparse regularization could indeed circumvent the possible ill-posedness caused by more damage parameters, refined elements for the UDP step is also possible in the proposed damage identification approach, which would be illustrated in the following numerical examples.

#### 4. Numerical simulation

In the following, three numerical simulations are used to test the proposed sparse-regularized min-CRE approach using FRF data. Damage identification results obtained by three identification approaches are compared in Section 4.1 and Section 4.2, namely the min-CRE approach with sparse regularization (C1), the sensitivity approach with Tikhonov regularization (S2) and the sensitivity approach with sparse regularization (S1). The advantage of being efficient for the proposed min-CRE approach is strongly substantiated. The example in Section 4.1 further considers some modeling errors in the mass matrix so as to testify the robustness of the identification results. Section 4.3 shows that the sparse regularization can significantly improve the accuracy of the identification results for a more general three-dimensional structure. For application of the iteration algorithm, the convergence tolerance is practically set to  $TOL = 1 \times 10^{-6}$ .

##### 4.1. A simply supported beam structure

In this example, a simply supported beam is utilized to compare the accuracy and efficiency between the proposed min-CRE approach and sensitivity approaches with different regularization techniques. The total length of the beam is 1m and the mass-per-length and bending stiffness are estimated as 1kg/m and  $1N \cdot m^2$ , respectively. As with finite element modelling, the beam is uniformly divided into 16 Euler-Bernoulli beam elements with 17 nodes each

**Table 1** Summary of the proposed AM method

Initial algorithm setting
<ul style="list-style-type: none"> <li>○ set initial damage parameters <math>\tilde{\boldsymbol{\theta}}_{(0)} = \tilde{\boldsymbol{\theta}}_0</math> as those of the intact structure</li> <li>○ set values of the maximum threshold setting rank <math>l_{max}</math> and the discriminating ratio <math>\alpha</math> for the threshold setting method</li> <li>○ define the convergence tolerance <b>TOL</b> and the maximum number of iterations <math>Z_{max}</math></li> <li>○ load the measured FRF data</li> </ul>
Alternating minimization approach (for $j = 1 : Z_{max}$ )
<ul style="list-style-type: none"> <li>○ Refer to the UMF step in Section 3.2 to obtain the updating mechanical field <math>(\tilde{\mathbf{q}}, \tilde{\mathbf{u}}^U)_{(j)}^T = \mathbf{L}(\tilde{\boldsymbol{\theta}}_{(j-1)})^{-1} \mathbf{S}(\tilde{\boldsymbol{\theta}}_{(j-1)})</math></li> <li>○ Choose the optimal regularization parameter <math>\lambda_{est}</math> according to the threshold setting method in Section 3.4 from <ul style="list-style-type: none"> <li>– for <math>e = 1 : N</math></li> <li>– <math>a_e = \int_{\Omega_e} \frac{r_1}{2} (\mathbf{B}_1 \tilde{\mathbf{u}}_{(j)}^e)^T \mathbf{D}_e (\mathbf{B}_1 \tilde{\mathbf{u}}_{(j)}^e) d\Omega</math>,</li> <li>– <math>b_e = \int_{\Omega_e} \frac{r_1}{2} (\mathbf{N}_2 \tilde{\mathbf{q}}_{(j)}^e)^T (\mathbf{D}_e)^{-1} (\mathbf{N}_2 \tilde{\mathbf{q}}_{(j)}^e) d\Omega</math></li> <li>– <math>\Lambda_e = \frac{1}{\Delta^e} (b_e - a_e)</math>, end for</li> <li>– <math>\lambda_{est} = \text{TSM}(\mathbf{\Lambda}, l_{max}, \alpha)</math></li> </ul> </li> <li>○ Refer to the UDP step in Section 3.3 to obtain the updating damage parameter <math>\theta_{e(j)}</math> for each element: <ul style="list-style-type: none"> <li>– if <math>\lambda_{est} &lt; \Lambda_e</math> then <math>\theta_{e(j)} = \sqrt{\frac{b_e}{a_e + \lambda_{est} \Delta^e}}</math>,</li> <li>– else if <math>\lambda_{est} &lt; -\Lambda_e</math> then <math>\theta_{e(j)} = \sqrt{\frac{b_e}{a_e - \lambda_{est} \Delta^e}}</math>,</li> <li>– else <math>\theta_{e(j)} = \theta_{e0} = 1</math></li> </ul> </li> <li>○ Convergence criterion <ul style="list-style-type: none"> <li>– if <math>\  \tilde{\boldsymbol{\theta}}_{(j)} - \tilde{\boldsymbol{\theta}}_{(j-1)} \  / \  \tilde{\boldsymbol{\theta}}_{(0)} \  \leq \text{TOL}</math> break.</li> </ul> </li> </ul>

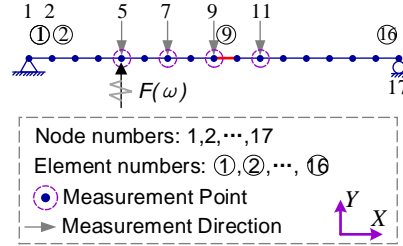


**Figure 2** Model of simply supported beam structure

with two degrees of freedom (see **Figure 2** for more details). The damage scenario admits the damage in element 9 with 20% stiffness reduction. The measurement points are chosen to be node 5, 7, 9 and 11 (Y direction only). The selected frequency range is simply chosen to be  $[1, 80]$ Hz with 1Hz intervals. For a more complicated model, an appropriate choice of the selected frequency range could improve the identification results greatly. Detailed selecting rules are discussed in Section 4.2. The measured FRF data at  $k$ th selected excitation frequency is obtained from simulation with addition of the measurement noise as follows,

$$\text{noise}_k(s) = \text{randn} \cdot a \cdot d_k(s), k = 1, 2, \dots, m \quad (27)$$

where  $\text{randn}$  is the normal distribution with zero mean and unit deviation,  $a$  is the applied noise level and  $d_k(s)$  is the measurement FRF data at certain position  $s$ . Noise level of 10% (Signal-to-Noise-Ratio, SNR=10dB) is considered in this example. For excitation, an unit harmonic load as shown in **Figure 2** is enforced at node 5.

#### 4.1.1. On choice of $(l_{\max}, \alpha)$ in the threshold setting method

To have an impression on how the maximum threshold setting rank  $l_{\max}$  and the discriminating ratio  $\alpha$  work in the threshold setting method, different choices of  $(l_{\max}, \alpha)$  for damage identification in different noise levels are studied herein and detailed results are displayed in **Figure 3**. On one hand, the identification process tends to be reasonably robust for a broad selection of  $(l_{\max}, \alpha)$  with appropriate ranges of  $\alpha \in [2, 50]$  and  $l_{\max} \in [2, 10]$  for the case with low level

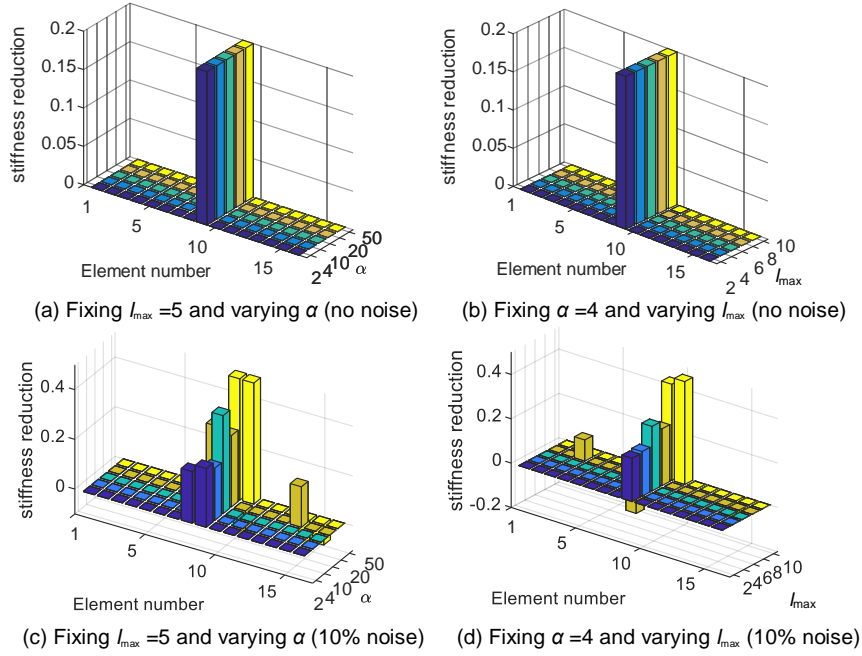


**Figure 3** Damage identification results under different choice of  $(l_{\max}, \alpha)$

of noise (**Figure 3(a), (b)**). On the other hand, the choice of  $(l_{\max}, \alpha)$  should be paid more attention for the case with high level of noise (**Figure 3(c), (d)**). Damage locations are badly identified for  $\alpha = 2$  and  $\alpha \geq 20$ . This means that the discriminating ratio  $\alpha$  should not be too small or too large. In terms  
 300 of the maximum threshold setting rank  $l_{\max}$ ,  $l_{\max} \geq 8$  leads to the failure of damage identification, indicating that  $l_{\max}$  shall not be too large. As a result, in the following of this example, the threshold parameters are reasonably fixed at  $l_{\max} = 5$ ,  $\alpha = 4$ .

#### 4.1.2. Comparison to the results by sensitivity-based algorithms

305 In this section, the following sensitivity-based algorithm, representing probably the most widely used techniques on the use of FRF data is considered.

Normally, the damage identification process based on the sensitivity approach is formulated as minimization of the following objective function-weighted

least squares of the error in measured quantities,

$$\arg \min \|\hat{\mathbf{R}} - \mathbf{R}(\boldsymbol{\theta})\|_{\mathbf{W}}^2 \quad (28)$$

where  $\hat{\mathbf{R}}$  and  $\mathbf{R}(\boldsymbol{\theta})$  denotes the measured and analytically predicted outputs respectively.  $\mathbf{W}$  is the positive definite weight matrix. Linearization of the above non-linear problem (28) at given  $\bar{\boldsymbol{\theta}}$  for iterative method is as follows

$$\hat{\mathbf{R}} - \mathbf{R}(\boldsymbol{\theta}) = \Delta\mathbf{R}(\bar{\boldsymbol{\theta}}) - \mathbf{S}(\bar{\boldsymbol{\theta}})\Delta\boldsymbol{\theta} \quad (29)$$

where  $\Delta\boldsymbol{\theta} := \boldsymbol{\theta} - \bar{\boldsymbol{\theta}}$  is the update of  $\boldsymbol{\theta}$ ,  $\Delta\mathbf{R}(\bar{\boldsymbol{\theta}}) := \hat{\mathbf{R}} - \mathbf{R}(\bar{\boldsymbol{\theta}})$  is the residual and  $\mathbf{S}(\bar{\boldsymbol{\theta}})$  is the response sensitivity matrix. For the method using frequency response function, the mathematical formulation of  $\mathbf{R}(\boldsymbol{\theta})$  and the  $e$ th column of sensitivity matrix  $\mathbf{S}$  are often expressed as[39]:

$$\mathbf{R}(\boldsymbol{\theta}) = [-\omega^2\mathbf{M}(\boldsymbol{\theta}) + \mathbf{K}(\boldsymbol{\theta})]\hat{\mathbf{u}}^M \quad (30)$$

$$\mathbf{S}_e = \left. \frac{\partial\mathbf{R}(\boldsymbol{\theta})}{\partial\theta_e} \right|_{\boldsymbol{\theta}=\bar{\boldsymbol{\theta}}} = \left[ -\omega^2 \frac{\partial\mathbf{M}}{\partial\theta_e} + \frac{\partial\mathbf{K}}{\partial\theta_e} \right]_{\boldsymbol{\theta}=\bar{\boldsymbol{\theta}}} \hat{\mathbf{u}}^M \quad (31)$$

where  $\hat{\mathbf{u}}^M$  represents the measured frequency-domain displacement response. Static condensation is needed so as to condense the above equation to the measured degrees of freedom and the weighting matrix  $\mathbf{H}(\omega, \bar{\boldsymbol{\theta}})$ , the frequency response function matrix should also be considered so as to reduce the bias on the estimated parameters. To circumvent the ill-posed problem, regularization is required. Objective function, solution method for each iteration and regularization parameter estimation method for different regularization types are briefly summarized in **Table 2**.

The final identification results are presented in **Figure 4**. As is seen, all of these three approaches can well identify the damage location and extent in the beam through of 10% noise level, except that false positions, although with minor degree, are also observed by the sensitivity approach with Tikhonov regularization (S2). Many researches have shown that Tikhonov regularization tends to produce over-smooth solutions because the quadratic regularizer cannot recover the sparse features of the solution.

As regards the corresponding convergence property in **Table 3**, it is shown that the computational effort necessary to solve C1(0.51s) is much less than the sensitivity approaches(4.89s-899.47s), although it takes more steps for C1 to get  
 325 convergent. This advantage attributes to the inherent decoupling nature of the CRE function with respect to the damage parameters, making every parameter-update-step solved as a series of single-variable optimization problems. It should be noted that due to the lack of closed-form solution for regularization parameter estimation, the computational time for S1 is huge(899.47s). For S1 with  
 330 unknown  $\lambda$ , an appropriate range of  $\lambda(2.9 - 5.4)$  is picked up by achieving balance between the residual norm and solution norm[29] as shown in **Figure 5(b)**. With the properly chosen or experienced-based  $\lambda$ , the computational cost of S1 could be reduced significantly(4.89s).

#### 4.1.3. Considering modeling errors

335 With respect to the modeling errors, simple mass modeling errors are added to the simulated beam structure. To do so, the exact mass density of element 2, 3 and 12, which are involved into the generation of the measured FRF data through simulation, are changed to 1.05kg/m, 1.05kg/m and 0.95kg/m respectively, while the mass density for damage identification are still set to  
 340 be 1kg/m as before. Noise level of 10% is also added into the measured FRF data. The identification results obtained by the three approaches are shown in **Figure 6**. As could be seen, the present approach (C1) could still identify the damage location clearly, although with a less satisfactory damage extent assessment. However, this bias can be further revised if needed by simply fixing the  
 345 damage location and optimizing the extent to match the observed changes. For the sensitivity-based approaches (S2&S1), the modelling errors may deteriorate the damage identification if no additional improvement, such as optimizing the weight matrix through the model error covariance[40], is enforced.

**Table 2** Sensitivity-based identification approaches with different regularizations

Approach	Objective function for each iteration	Solution method for each iteration	Parameter estimation method
S2[39]	$\  \Delta \mathbf{R}(\bar{\theta}) - \mathbf{S}(\bar{\theta}) \Delta \theta \ _{\mathbf{W}}^2 + \lambda \  \Delta \theta \ _2^2$	closed-form solution $\Delta \theta = [\mathbf{S}(\bar{\theta})^T \mathbf{W} \mathbf{S}(\bar{\theta}) + \lambda \mathbf{I}]^{-1} \mathbf{S}(\bar{\theta})^T \mathbf{W} \Delta \mathbf{R}(\bar{\theta})$	L-curve method
S1[22]	$\  \Delta \mathbf{R}(\bar{\theta}) - \mathbf{S}(\bar{\theta}) \Delta \theta \ _{\mathbf{W}}^2 + \lambda \  \Delta \theta \ _1$	Primal-dual interior point method <i>Newton's method (again iterative) proceeds</i>	Using residual and solution norms[29]

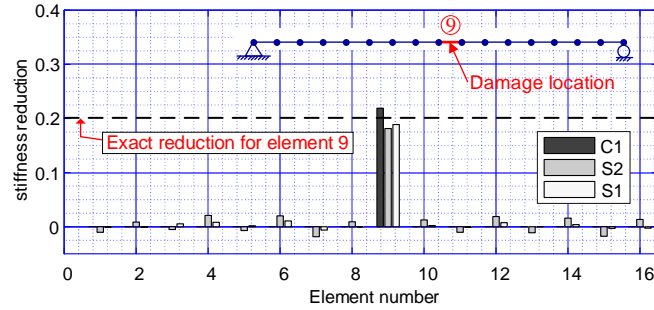


**Figure 4** Stiffness reduction for each element using different approaches

**Table 3** Convergence property for different identification approaches

Approach	Numbers of iterations	Total computation time (s)
C1	24	0.51
S2	6	5.41
S1	-	899.47
S1(with known $\lambda$ )	9	4.89

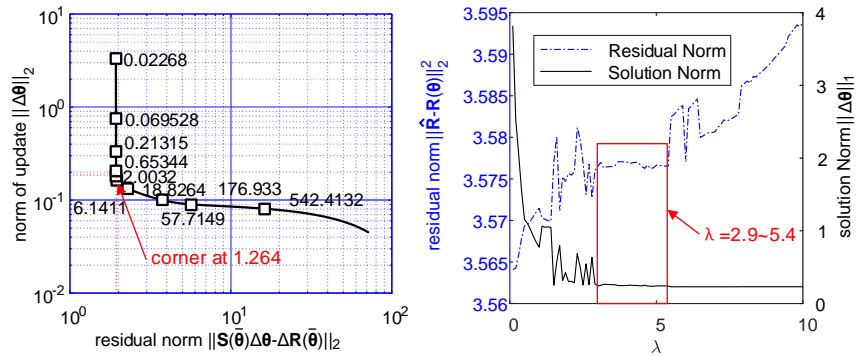


**Figure 5** Regularization parameter selection: (a) L-curve method for Tikhonov regularization; (b) using residual and solution norms for sparse regularization

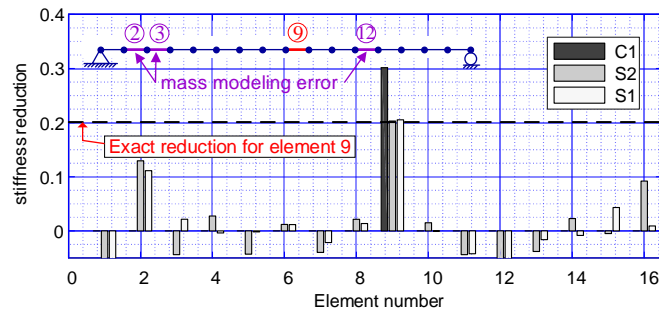


**Figure 6** Stiffness reduction for each element using different approaches with mass modeling errors

#### 4.2. A plane frame structure

A plane frame structure as shown in **Figure 7** is studied in the second example (see reference[9] for detailed explanation on the target structure). The height and width of the frame are  $H = 1.2\text{m}$  and  $L = 0.6\text{m}$ , respectively, and the rectangular cross-sectional dimensions are  $b = 0.01\text{m}$  and  $h = 0.02\text{m}$  with the inertial moment for planar bending  $I = 6.67 \times 10^{-9}\text{m}^4$  and area  $A = 2 \times 10^{-4}\text{m}^2$ . For the undamaged frame, the mass density of the material is  $\rho = 2.7 \times 10^3\text{kg/m}^3$  and the Young's modulus is  $E = 6.9 \times 10^{10}\text{N/m}^2$ . The plane frame analysis model consists of 88 Euler-Bernoulli beam elements with 89 nodes, each with three degrees of freedom. This finer numerical model is used to obtain the mechanical field for the UMF step so that the discretization error caused by finite element model could be ignored. For the UMP step, the structure is divided in 11 sets of elements (see **Figure 7(b)**) and the identification procedure updates the 11 element parameters independently. A single harmonic load is applied in the  $x$ -direction of node 2. The FRF data are obtained by the discrete Fourier transform(DFT) of the corresponding numerical simulated accelerations (see **Figure 9** for the FRF data of node 2). Twelve damage scenarios, including single and multiple, small and large damage, unpolluted and polluted measurements are taken into account, as listed in **Table 4**, where Nil stands for no noise. The measurement locations and the corresponding directions are also illustrated in **Table 4** and **Figure 8**. Herein, the stiffness parameters  $\{\theta_e, e = 1, 2, \dots, N\}$ , standing for the Young's modulus of each element set, is identified and the identified results in the percentage error forms are presented as

$$\text{Relative error}(\%) = \frac{\theta_e^{id} - \theta_e}{\theta_e} \times 100\% \quad (32)$$

350 where  $\theta_e^{id}$  and  $\theta_e$  are identified and true values of the stiffness parameter for each element set, respectively. Noise level of 10% (SNR=10dB) is added to the measurements primarily.

Several practical rules for selecting excitation frequencies are

- Excitation frequencies should not be selected at resonance frequencies to

355

prevent resonance phenomena and high sensitivity to noise.

- Dynamic response of the target structure is more sensitive to damages for frequency points close to resonances than points far from resonances. Therefore, excitation frequency points near resonance frequencies are recommended for measurement[32].
- 360 • Although the response of the target structure in higher frequency ranges, which excites higher mode shapes, is more sensitive to damages, numerical analysis results are shown with less accuracy than those in lower frequency ranges[41].
- Using more frequency ranges corresponding to different resonance frequencies could improve the identification accuracy while using more frequency points near one resonance frequency seems to have no significantly effect on the results for lower noise level cases.
- 365 • For higher levels of noise, presence of more frequency points near certain resonance frequency can result in a robust identification.

370 Based on these rules, the selected frequency ranges are given in **Table 5** and the sampling frequency stepping size in each frequency range is 4Hz. Consequently, identification results of each scenario are obtained using 50 frequency points.

As is observed in **Table 6** with the relative error defined in equation (32), for the single damage scenarios 1-6, the proposed approach could provide satisfied identification results: the maximum relative error does not exceed 0.02%  
375 in the case of no noise and 1% in the case of 10% noise. Only the horizontal acceleration response at nodes 2 and 9 is measured herein. For the multiple damages scenarios 7-12, the horizontal frequency response at node 4 and the vertical acceleration response at node 7 are additionally measured. The identification by the min-CRE approach can well identify the damage locations as well  
380 as extents with a maximum relative error 0.01% in the case of no noise and 3.7% in the case of 10% noise. Compared with the results in the reference[9], which

used an enhanced response sensitivity approach with the Tikhonov regularization under the same measurement degrees of freedom, identification results of the min-CRE approach with the sparse regularization demonstrated the superiority for all of the 12 scenarios. Most of this superior identification accuracy is attributed to the enforced sparse regularization: the sparse regularization yields sparse damages that are more compatible with practical damage patterns, while the Tikhonov-regularized damage identification does not result in sparse solutions, which typically have non-zero relative errors associated with all damage parameters[42]. All coincide with the existed observations where replacement of the Tikhonov regularization by the sparse regularization can indeed improve the identification accuracy and robustness for damage identification.

To get a better picture on the effectiveness of the sparse regularization, detailed identification results for scenario 5 are shown in **Figure 10**. It is shown that stiffness reduction is obtained based on  $\hat{\theta}_e$  in equation (??), where no sparsity term is introduced. Obviously, when there is no measurement noise, using or not using sparse regularization would lead to the same good identification results. However, it is almost impossible to get to the reasonable identification results for the case without sparse regularization when measurement noise is enforced. It is clear that the sparse regularization greatly improves the identifiability and robustness of the CRE-approach. Furthermore, to visualize how the sparse-regularized min-CRE approach proceeds, the iterative procedure for the scenario 5 is shown in **Figure 11**. On the other hand, **Figure 12** compares the evolution of the constitutive relation error(CRE) for each of the iterative step with different levels of noise (0%, 5%, 10% and 20%) for damage scenario 5. As is observed, the error decreases with the number of iterations increases, verifying the convergence of the present method.

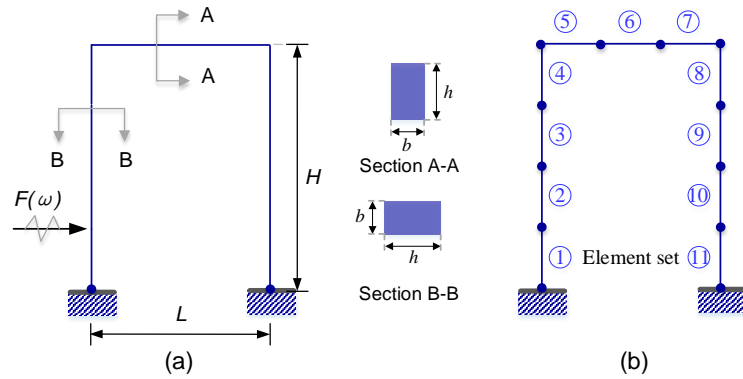


**Figure 7** Model of plane frame structure: (a)Geometry, (b)Element sets

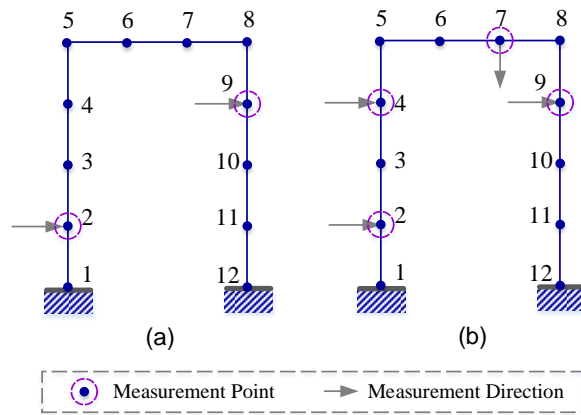
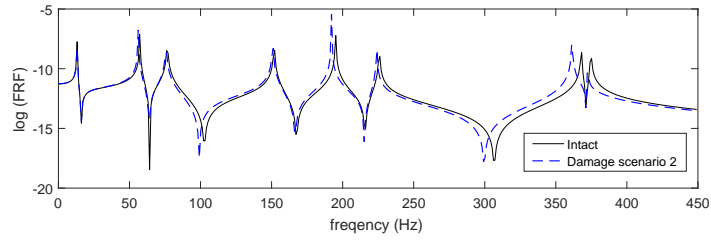
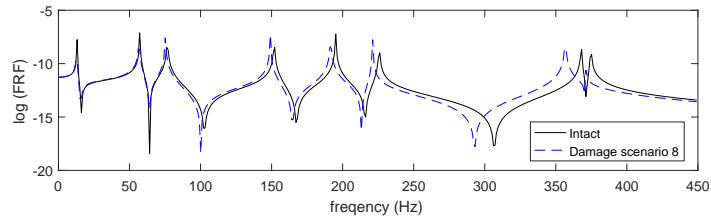


**Figure 8** Measurement points and directions



(a) Scenario 2



(b) Scenario 8

**Figure 9** FRF of the plane frame structure in the  $x$ -direction of node 2

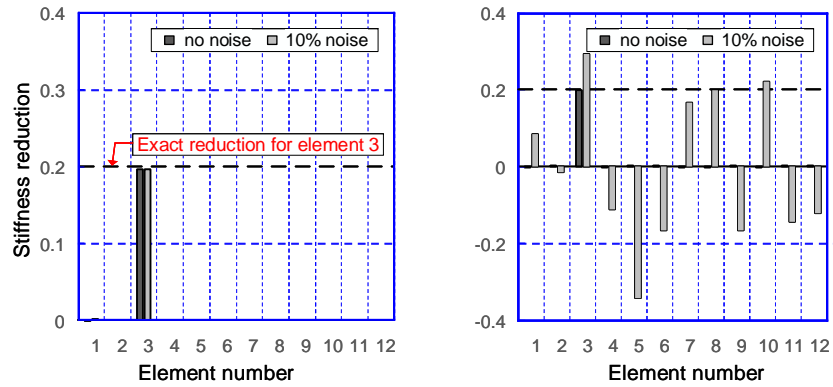


**Figure 10** Stiffness reduction for scenario 2/5: (a) the min-CRE approach with sparse regularization; (b) the min-CRE approach without sparse regularization

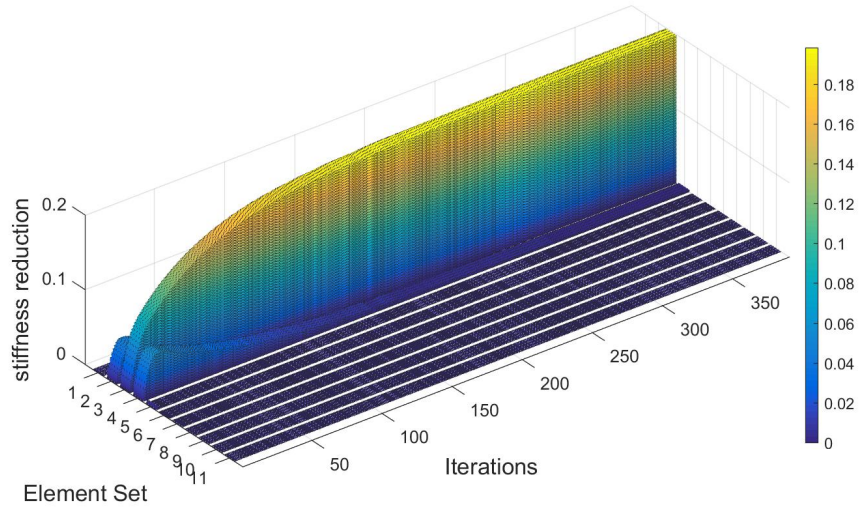


**Figure 11** Damage identification procedure for scenario 5 of the plane frame structure

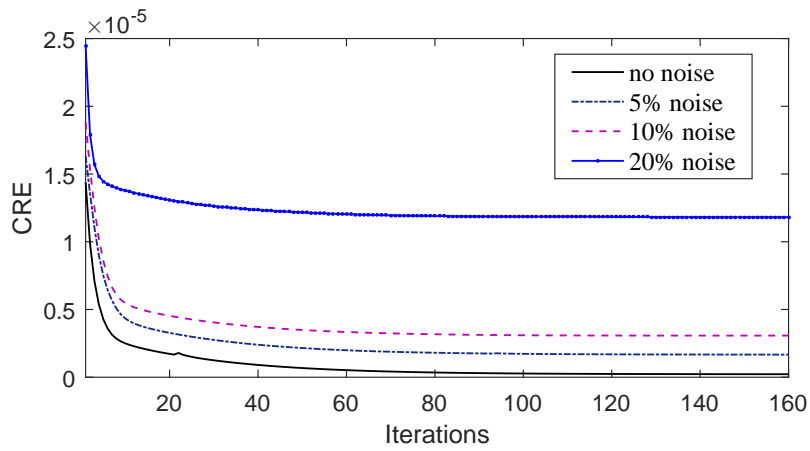


**Figure 12** CRE vs iterations for damage scenario 5 with different levels of noise

**Table 4** Damage scenarios for plane frame structure

Damage scenario	Damage location	Reduction in		
scenario	(element set no.)	elastic modulus (%)	Noise (%)	Measurement
1	3	10	Nil	$\ddot{u}_2, \ddot{u}_9$
2	3	20	Nil	$\ddot{u}_2, \ddot{u}_9$
3	3	40	Nil	$\ddot{u}_2, \ddot{u}_9$
4	3	10	10	$\ddot{u}_2, \ddot{u}_9$
5	3	20	10	$\ddot{u}_2, \ddot{u}_9$
6	3	40	10	$\ddot{u}_2, \ddot{u}_9$
7	4,5	10,5	Nil	$\ddot{u}_2, \ddot{u}_4, \ddot{u}_9, \ddot{v}_7$
8	4,5	20,25	Nil	$\ddot{u}_2, \ddot{u}_4, \ddot{u}_9, \ddot{v}_7$
9	4,5	50,50	Nil	$\ddot{u}_2, \ddot{u}_4, \ddot{u}_9, \ddot{v}_7$
10	4,5	10,5	10	$\ddot{u}_2, \ddot{u}_4, \ddot{u}_9, \ddot{v}_7$
11	4,5	20,25	10	$\ddot{u}_2, \ddot{u}_4, \ddot{u}_9, \ddot{v}_7$
12	4,5	50,50	10	$\ddot{u}_2, \ddot{u}_4, \ddot{u}_9, \ddot{v}_7$

**Table 5** Frequency ranges for scenarios 1-12 of plane frame structure (Hz)

Scenario	1&4	2&5	3&6	7&10	8&11	9&12
Frequency ranges	50-82	50-82	46-82	46-74	50-82	50-82
(4Hz intervals)	143-147	143-147	139-143	139-143	139-143	127-135
	157-161	153-157	157-161	157-161	157-161	149-161
	169-185	165-185	169-181	169-185	169-185	165-177
	199-215	195-219	195-211	199-219	195-215	187-203
	230-262	226-258	226-258	230-262	226-258	215-251
	316-352	316-352	308-336	316-352	316-348	300-316
	382-410	378-394	386-422	382-410	382-410	378-402

**Table 6** Error in the Young's modulus for each element set of damage scenarios 1-12

Damage scenario	Error (%) in each element set by min-CRE approach											Error (%) in each element set by sensitivity approach										
	1	2	3	4	5	6	7	8	9	10	11	1	2	3	4	5	6	7	8	9	10	11
1	-0.01	0.00	0.01	0.00	0.00	0.00	0.00	0.00	0.00	0.00	0.00	0.02	-0.10	-0.12	0.20	0.23	-0.05	-0.34	-0.05	0.26	0.00	-0.07
2	-0.01	0.00	0.02	0.00	0.00	0.00	0.00	0.00	0.00	0.00	0.00	0.07	-0.29	-0.43	0.59	0.75	-0.17	-1.38	0.01	0.96	-0.07	-0.21
3	0.00	0.00	0.01	0.00	0.00	0.00	0.00	0.00	0.00	0.00	0.00	0.02	-0.19	-0.25	0.60	0.25	-0.23	-1.59	0.31	1.05	-0.24	-0.14
4	0.00	0.00	-0.18	0.00	0.00	0.00	0.00	0.00	0.00	0.00	0.00	-0.08	1.81	0.82	-0.80	-2.70	-0.88	1.49	-0.32	-0.58	-1.10	0.83
5	-0.27	0.00	0.23	0.00	0.00	0.00	0.00	0.00	0.00	0.00	0.00	0.09	1.55	0.42	-0.44	-2.20	-1.12	1.47	0.34	0.59	-1.87	0.06
6	-1.00	0.00	0.45	0.00	0.00	0.00	0.00	0.00	0.00	0.00	0.00	0.02	0.73	0.52	1.70	-2.83	-0.85	-0.70	-0.21	2.06	-2.00	-0.21
7	0.00	0.00	-0.01	0.00	0.01	0.01	0.00	0.00	0.00	0.00	0.00	0.10	-0.26	-0.33	0.23	0.76	-0.04	-0.32	-0.24	0.29	0.13	-0.17
8	0.00	0.00	-0.01	0.00	0.01	0.01	0.00	0.00	0.00	0.00	0.00	0.10	-0.19	-0.35	0.14	0.75	-0.04	-0.20	-0.33	0.11	0.22	-0.10
9	0.00	0.00	0.00	0.01	0.00	0.00	0.00	0.00	0.00	0.00	0.00	0.02	-0.03	-0.10	-0.03	0.26	-0.01	0.13	-0.18	-0.11	0.11	0.00
10	0.00	0.00	0.00	1.01	2.57	0.00	-1.98	0.00	0.00	0.00	0.00	-0.61	0.95	1.83	-1.01	-2.71	0.66	0.73	0.36	-2.29	0.13	1.27
11	0.00	0.69	-1.74	-0.81	3.69	0.00	-1.70	0.00	0.00	2.60	0.00	-0.99	1.63	1.36	-2.25	-0.78	1.42	1.28	-0.76	-3.93	0.98	2.23
12	-1.26	0.00	0.00	3.42	-3.71	0.00	0.00	0.00	0.00	0.00	0.00	0.27	-0.52	-2.15	-0.19	4.82	-0.66	3.02	-2.22	-0.46	0.22	-0.45

### 4.3. A three-dimensional frame structure

410 The performance of the presented approach is also illustrated by using a three-dimensional structure. It is a 2-story, 1-bay by 1-bay frame structure as shown schematically in **Figure 13**. Parameters of this frame are: height  $H = 4\text{m}$ , length  $L = 4\text{m}$ , width  $B = 3\text{m}$ , rectangular cross-section  $h \times b = 0.01\text{m} \times 0.01\text{m}$ , intact Young's modulus  $E = 2.1 \times 10^{11}\text{pa}$ , Poisson's ratio  $\nu = 0.3$  and mass density  $\rho = 7860\text{kg/m}^3$ . Shear modulus  $G$  for this structure is taken as  $E/(2(1 + \nu))$  herein. Simulated dynamic FRF data are used in this study. Two synthetic harmonic load is applied at node 7 and node 9. Node 5(x,y direction) and node 7(x,y direction) are selected as two measurement points. These input data are contaminated by normal distribution noise with the noise level 10% (SNR=10dB) according to equation (27). The selected frequency range in this example is  $[0.4, 4.5]\text{Hz}$  with  $0.05\text{Hz}$  intervals. Some of the excitation frequencies are ignored based on the selection rules as stated in Section 4.2. To clearly understand the spatial motion over the entire model, displacement fields for different frequencies are depicted in **Figure 14**.

425 Damages are enforced by reducing the Young's modulus  $E$  to 70% in element 1 ( $\theta_1 = 0.7$ ) and 80% in element 16 ( $\theta_{16} = 0.8$ ). As shown in **Figure 15(a)**, good identification performance is achieved when noise level is up to 10%. The optimal regularization parameters are  $\lambda_{\text{est}} = 1.45422 \times 10^{-13}$  for the no noise case and  $\lambda_{\text{est}} = 3.72452 \times 10^{-13}$  for the 10% noise case. Again, identification results with and without sparsity are additionally compared in **Figure 15**. From the results of the identified stiffness reduction under the measurement noise and without the sparse regularization (**Figure 15(b)**), damage locations and extents became almost unidentifiable, while the sparse regularization substantially improves the accuracy and robustness of the identification procedure (**Figure 15(a)**). The proposed damage identification approach with sparsity is shown to be well applicable to the identification in 3D frames.

To show the convergence of the proposed sparse-regularized min-CRE approach, filled contour plot of the damage parameters  $\tilde{\theta}$  was drawn in **Figure 16**. As it is seen, damages are identified after 35 steps, verifying the convergence

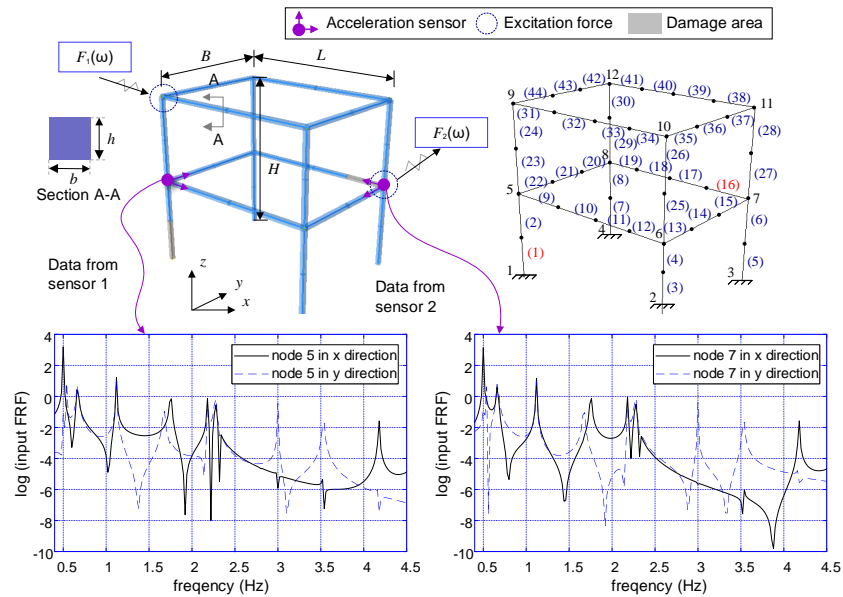


**Figure 13** Schematic diagram showing the numerical structure and the directions of system output measurements and input excitations

440 of the present method. Algorithm without sparsity would encounter divergence or convergence difficulty with the same amount of input measurement data. This phenomenon is attributable to the fact that sparse regularization provides a flexible and parsimonious reconstructing process for high-dimensional model parameters from limited incomplete input data.

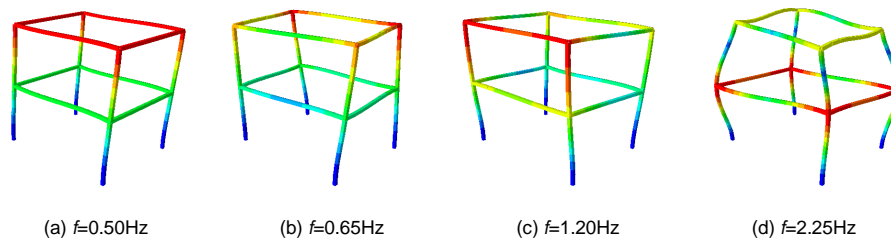


**Figure 14** Displacement fields for different frequency

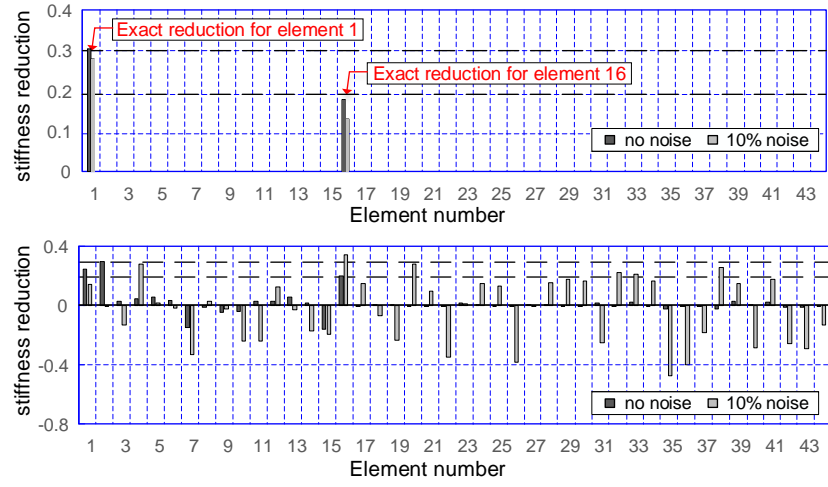


**Figure 15** Stiffness reduction for each element: (a) the min-CRE approach with sparse regularization; (b) the min-CRE approach without sparse regularization

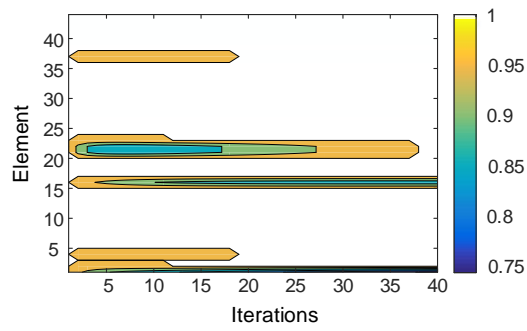


**Figure 16** Contour plot of damage parameters for each element

## 445 5. Conclusions

This research is focused on the damage identification approach with incom-  
pleted frequency response data using the minimum constitutive relation error  
(min-CRE) principle and the sparse regularization. The identification process  
is a nonlinear optimization problem and the corresponding objective function is  
450 set to measure the residual of the constitutive equations connecting the admis-  
sible stress field and the admissible displacement field. Numerical examples are  
conducted to verify the present approach and the results show that:

1. The present damage identification approach performs well in both dam-  
age localization and extent assessment for 2D/3D frame structures with  
455 incomplete frequency response data.
2. The AM method could effectively tackle the nonlinear optimization prob-  
lem.
3. The sparse regularization obviously improves the accuracy and robustness  
of the damage identification results.
- 460 4. The sparse regularization along with the CRE objective function is shown  
to be more accurate than the Tikhonov regularization along with the sen-  
sitivity identification approach.
5. The proposed threshold setting method could be used to determine the  
sparse regularization parameter automatically and efficiently.
- 465 6. The proposed approach is found to be much more efficient and less sen-  
sitive to the mass modeling errors than the sensitivity-based approaches  
(with the Tikhonov regularization or with the sparse regularization).

## APPENDIX

### A.1. The displacement finite element

The auxiliary local nodal displacements  $(u_x^i, u_y^i, u_z^i, \theta_x^i, \theta_y^i, \theta_z^i)$  (3 translations  
and 3 rotation) at an arbitrary node  $i$  are naturally selected to obtain the

admissible displacement solution first. Thus, for an arbitrary element  $e$  with two nodes  $i, j$ , the discretized displacement field  $(w_x^e, w_y^e, w_z^e, \theta_x^e)$  as shown in **Figure A.1** constructed by linear Lagrange interpolation for  $(w_x^e, \theta_x^e)$  and cubic Hermit interpolation for  $(w_y^e, w_z^e)$  based on the corresponding local nodal displacements  $(u_x^i, u_y^i, u_z^i, \theta_x^i, \theta_y^i, \theta_z^i)$  and  $(u_x^j, u_y^j, u_z^j, \theta_x^j, \theta_y^j, \theta_z^j)$ , is expressed as

$$\begin{pmatrix} w_x^e \\ w_y^e \\ w_z^e \\ \theta_x^e \end{pmatrix} = \mathbf{\Phi}_u^e \tilde{\mathbf{u}}_L^e, \quad \tilde{\mathbf{u}}_L^e := [u_x^i, u_y^i, u_z^i, \theta_x^i, \theta_y^i, \theta_z^i, u_x^j, u_y^j, u_z^j, \theta_x^j, \theta_y^j, \theta_z^j]^T$$

$$\mathbf{\Phi}_u^e := \begin{pmatrix} N_1 & 0 & 0 & 0 & 0 & 0 & N_2 & 0 & 0 & 0 & 0 & 0 \\ 0 & H_1 & 0 & 0 & 0 & H_2 & 0 & H_3 & 0 & 0 & 0 & H_4 \\ 0 & 0 & H_1 & 0 & -H_2 & 0 & 0 & 0 & H_3 & 0 & -H_4 & 0 \\ 0 & 0 & 0 & N_1 & 0 & 0 & 0 & 0 & 0 & N_2 & 0 & 0 \end{pmatrix} \quad (\text{A-1})$$

where the polynomial interpolation functions  $N_1, N_2, H_1, H_2, H_3, H_4$  are of the following forms,

$$\begin{cases} N_1(\xi) = \frac{1-\xi}{2}, N_2(\xi) = \frac{1+\xi}{2} \\ \begin{cases} H_1(\xi) = \frac{1}{2}(\xi+2)(\xi-1)^2, H_2(\xi) = \frac{1}{4}(\xi+1)(\xi-1)^2 \frac{h^e}{2}, \\ H_3(\xi) = \frac{1}{2}(2-\xi)(\xi+1)^2, H_4(\xi) = \frac{1}{4}(\xi-1)(\xi+1)^2 \frac{h^e}{2}, \end{cases} \\ \xi = \frac{2(s-s_1^e)}{h^e} - 1 \end{cases} \quad (\text{A-2})$$

In order to perform the further assembling computation, the local nodal displacements  $\tilde{\mathbf{u}}_L^e$  need to be expressed in a common coordinate system or the global coordinate system. To this end, the relationship between local nodal displacements  $\tilde{\mathbf{u}}_L^e$  and global nodal displacements  $\tilde{\mathbf{u}}^e$  in element  $e$  is explored, pertaining to

$$\tilde{\mathbf{u}}_L^e = \mathbf{T}_u^e \tilde{\mathbf{u}}^e, \quad (\text{A-3})$$

where  $\mathbf{T}_u^e$  is the transformation matrix of the following form

$$\mathbf{T}_u^e = \begin{pmatrix} \mathbf{t} & \mathbf{0} & \mathbf{0} & \mathbf{0} \\ \mathbf{0} & \mathbf{t} & \mathbf{0} & \mathbf{0} \\ \mathbf{0} & \mathbf{0} & \mathbf{t} & \mathbf{0} \\ \mathbf{0} & \mathbf{0} & \mathbf{0} & \mathbf{t} \end{pmatrix} \quad (\text{A-4})$$

$$\mathbf{t} = \begin{pmatrix} \cos(x, \bar{x}) & \cos(x, \bar{y}) & \cos(x, \bar{z}) \\ \cos(y, \bar{x}) & \cos(y, \bar{y}) & \cos(y, \bar{z}) \\ \cos(z, \bar{x}) & \cos(z, \bar{y}) & \cos(z, \bar{z}) \end{pmatrix} \quad (\text{A-5})$$

470  $\mathbf{t}$  is the Direction Cosine Matrix (DCM) between local coordinate system ( $Oxyz$ ) and global coordinate system ( $O\bar{x}\bar{y}\bar{z}$ ).

For brevity, the displacement finite element approximation is designated as

$$\begin{pmatrix} w_x^e \\ w_y^e \\ w_z^e \\ \theta_x^e \end{pmatrix} = \mathbf{N}_1^e \tilde{\mathbf{u}}^e, \quad \mathbf{N}_1^e := \mathbf{\Phi}_u^e \mathbf{T}_u^e \quad (\text{A-6})$$

### A.2. The force finite element

In the force finite dimensional space, the discretized stress field ( $N_x^e, M_z^e, M_y^e, M_x^e$ ) (see **Figure A.2**) for an arbitrary element  $e$  should be constructed at first. Practically, this can be reached by setting

$$(N_x^e, M_z^e, M_y^e, M_x^e) = (N_x^{0e}, M_z^{0e}, M_y^{0e}, M_x^{0e}) + (N_x^{pe}, M_z^{pe}, M_y^{pe}, M_x^{pe}) \quad (\text{A-7})$$

where ( $N_x^{pe}, M_z^{pe}, M_y^{pe}, M_x^{pe}$ ) is the inhomogeneous part caused by the concentrated loads on Neumann boundary  $\partial\Omega_f$  and ( $N_x^{0e}, M_z^{0e}, M_y^{0e}, M_x^{0e}$ ) is the homogeneous part approximated by the following force element.

475

Auxiliary local nodal forces ( $N_x^i, V_y^i, V_z^i, M_x^i, M_y^i, M_z^i$ ) at an arbitrary node  $i$  are used to construct the homogeneous discretized stress field ( $N_x^0, M_z^0, M_y^0, M_x^0$ )

initially; that is, for element  $e$ ,  $(N_x^{0e}, M_z^{0e}, M_y^{0e}, M_x^{0e})$  are given by

$$\begin{aligned} (N_x^{0e}, M_z^{0e}, M_y^{0e}, M_x^{0e})^T &= \mathbf{\Phi}_q^e \tilde{\mathbf{q}}_{0L}^e, \\ \tilde{\mathbf{q}}_{0L}^e &:= [N_x^i, V_y^i, V_z^i, M_x^i, M_y^i, M_z^i, N_x^j, V_y^j, V_z^j, M_x^j, M_y^j, M_z^j]^T \\ \mathbf{\Phi}_q^e &:= \begin{pmatrix} N_1 & 0 & 0 & 0 & 0 & 0 & N_2 & 0 & 0 & 0 & 0 & 0 \\ 0 & -H_2 & 0 & 0 & 0 & H_1 & 0 & -H_4 & 0 & 0 & 0 & H_3 \\ 0 & 0 & H_2 & 0 & H_1 & 0 & 0 & 0 & H_4 & 0 & H_3 & 0 \\ 0 & 0 & 0 & N_1 & 0 & 0 & 0 & 0 & 0 & N_2 & 0 & 0 \end{pmatrix} \end{aligned} \quad (\text{A-8})$$

where  $\mathbf{\Phi}_q^e$  is the shape function matrix. Having gained  $(N_x^{0e}, M_z^{0e}, M_y^{0e}, M_x^{0e})$  in equation (A-8) via the auxiliary local nodal forces, the next is to shift into the usage of global nodal forces. To this end, the transformation matrix for the force finite element pertains to be

$$\mathbf{T}_q^e = \mathbf{H} \mathbf{T}_u^e \quad (\text{A-9})$$

where

$$\mathbf{H} = \begin{pmatrix} -\mathbf{I}_{6 \times 6} & \mathbf{0} \\ \mathbf{0} & \mathbf{I}_{6 \times 6} \end{pmatrix} \quad (\text{A-10})$$

Hence, the relationship between local element nodal forces  $\tilde{\mathbf{q}}_{0L}^e$  and global element nodal forces  $\tilde{\mathbf{q}}_0^e$  in terms of element  $e$  is given by

$$\tilde{\mathbf{q}}_{0L}^e = \mathbf{T}_q^e \tilde{\mathbf{q}}_0^e \quad (\text{A-11})$$

Next, the formulation of nodal equilibriums is utilized to find independent global nodal force (DOFs)  $\hat{\mathbf{q}}_0^e$ . Element nodal forces  $\tilde{\mathbf{q}}_0^{ei} = [F_x^{ei}, F_y^{ei}, F_z^{ei}, M_x^{ei}, M_y^{ei}, M_z^{ei}]^T$  of all  $r$  beams as well as reaction forces  $\mathbf{R}_G^i = [R_x^i, R_y^i, R_z^i, RM_x^i, RM_y^i, RM_z^i]^T$  adjacent to the objective node  $i$  in the directions of all the degrees of freedom are algebraically summed up as shown in **Figure A.3**. This is carried out for all nodes. The equilibrium equation for each node  $i$  is accordingly given by

$$\sum_{e=1}^r \tilde{\mathbf{q}}_0^{ei} + \mathbf{R}_G^i = \mathbf{0} \quad (\text{A-12})$$

Based on this equilibrium equation, dependent nodal forces  $\tilde{\mathbf{q}}_0^{ri}$  could be represented by independent global nodal forces  $\hat{\mathbf{q}}_0^{ei} := (\tilde{\mathbf{q}}_0^{ei}, e = 1, 2, \dots, r - 1, \mathbf{R}_G^i)$  for the node  $i$  in the sequel

$$\mathbf{n}\hat{\mathbf{q}}_0^{ei} = -\sum_{e=1}^{r-1} \tilde{\mathbf{q}}_0^{ei} - \mathbf{R}_G^i = \tilde{\mathbf{q}}_0^{ri} \quad (\text{A-13})$$

where  $\mathbf{n}$  stands for the linear combination of  $\{\tilde{\mathbf{q}}_0^{ei}, e = 1, 2, \dots, r - 1\}$  and  $\mathbf{R}_G^i$ . It should be noticed that homogeneous Neumann boundary conditions should be enforced on reaction forces  $\mathbf{R}_G^i$ , setting corresponding forces to be zero for different types of supports. Thus, one can obtain for an element  $e$  with an ending node  $i$  that

$$[F_x^{ei}, F_y^{ei}, F_z^{ei}, M_x^{ei}, M_y^{ei}, M_z^{ei}]^T = \mathbf{L}_i^e \hat{\mathbf{q}}_0^{ei} \quad (\text{A-14})$$

where

$$\begin{aligned} \mathbf{L}_i^e(3e - 2 : 3e, 3e - 2 : 3e) &= \mathbf{I}_{3 \times 3} \text{ for } e = 1, 2, \dots, r - 1 \\ \mathbf{L}_i^e &= \mathbf{n} \text{ for } e = r \end{aligned} \quad (\text{A-15})$$

Integrating Equations (A-8),(A-11) and (A-14), the force finite element approximation of  $(\hat{N}_h^e, \hat{M}_h^e)$  is established as

$$\begin{aligned} \begin{pmatrix} N_x^{0e} \\ M_z^{0e} \\ M_y^{0e} \\ M_x^{0e} \end{pmatrix} &= \Psi_q^e \hat{\mathbf{q}}_0^e = \mathbf{N}_2^e \tilde{\mathbf{q}}_0^e \\ \Psi_q^e &:= \mathbf{N}_2^e \begin{pmatrix} \mathbf{L}_i^e & \mathbf{0} \\ \mathbf{0} & \mathbf{L}_i^e \end{pmatrix} = \Phi_q^e \mathbf{T}_q^e \begin{pmatrix} \mathbf{L}_i^e & \mathbf{0} \\ \mathbf{0} & \mathbf{L}_i^e \end{pmatrix} \\ \tilde{\mathbf{q}}_0^e &= \begin{pmatrix} \mathbf{L}_i^e & \mathbf{0} \\ \mathbf{0} & \mathbf{L}_i^e \end{pmatrix} \hat{\mathbf{q}}_0^e = \begin{pmatrix} \mathbf{L}_i^e & \mathbf{0} \\ \mathbf{0} & \mathbf{L}_i^e \end{pmatrix} \begin{pmatrix} \hat{\mathbf{q}}_0^i \\ \hat{\mathbf{q}}_0^j \end{pmatrix} \end{aligned} \quad (\text{A-16})$$

Turning to the particular part  $(N_x^{pe}, M_z^{pe}, M_y^{pe}, M_x^{pe})$ , the external concentrated loads are directly involved. Assume that the concentrated loads  $\tilde{\mathbf{q}}_p^e := [F_{px}, F_{py}, F_{pz}, M_{px}, M_{py}, M_{pz}]^T$  are enforced on the left-hand side  $k = 1$  (or right-hand side  $k = 2$ ) of the element  $e$ . Under this circumstance,  $(N_x^{pe}, M_z^{pe},$

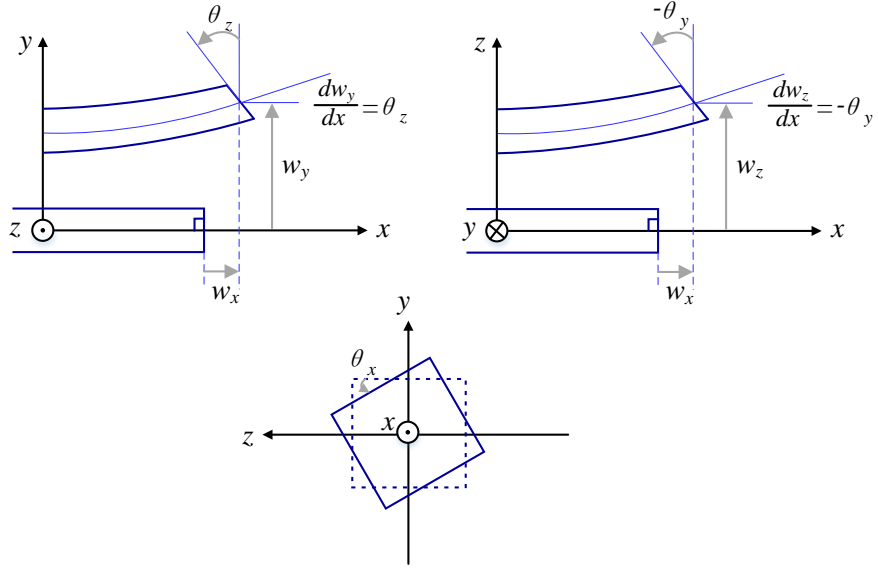


Figure A. .1 Basics of a displacement finite element  $e$

$M_y^{pe}, M_x^{pe}$ ) could be obtained by the interpolation matrix defined in equation (A-1) and transformation matrix defined in equation (A-9) as follows

$$\begin{pmatrix} N_x^{pe} \\ M_z^{pe} \\ M_y^{pe} \\ M_x^{pe} \end{pmatrix} = \mathbf{N}_2^e \tilde{\mathbf{q}}_p^e \quad (\text{A-17})$$

where  $\tilde{\mathbf{q}}_p$  collects all concentrated loads  $(F_{px}, F_{py}, F_{pz}, M_{px}, M_{py}, M_{pz})$ .

Finally, substituting Equation (A-16) and (A-17) into Equation (A-7) and simplifying, one can get

$$\begin{pmatrix} N_x^e \\ M_z^e \\ M_y^e \\ M_x^e \end{pmatrix} = \mathbf{N}_2^e \tilde{\mathbf{q}}_0^e + \mathbf{N}_2^e \tilde{\mathbf{q}}_p^e \quad (\text{A-18})$$

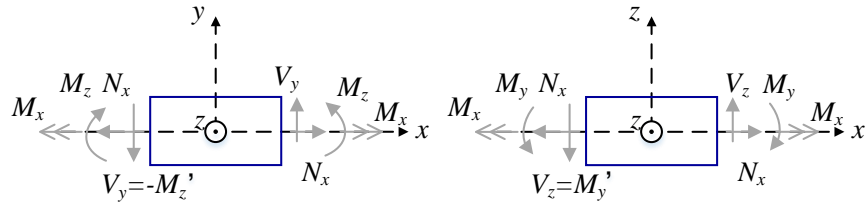


Figure A. .2 Basics of a force finite element  $e$

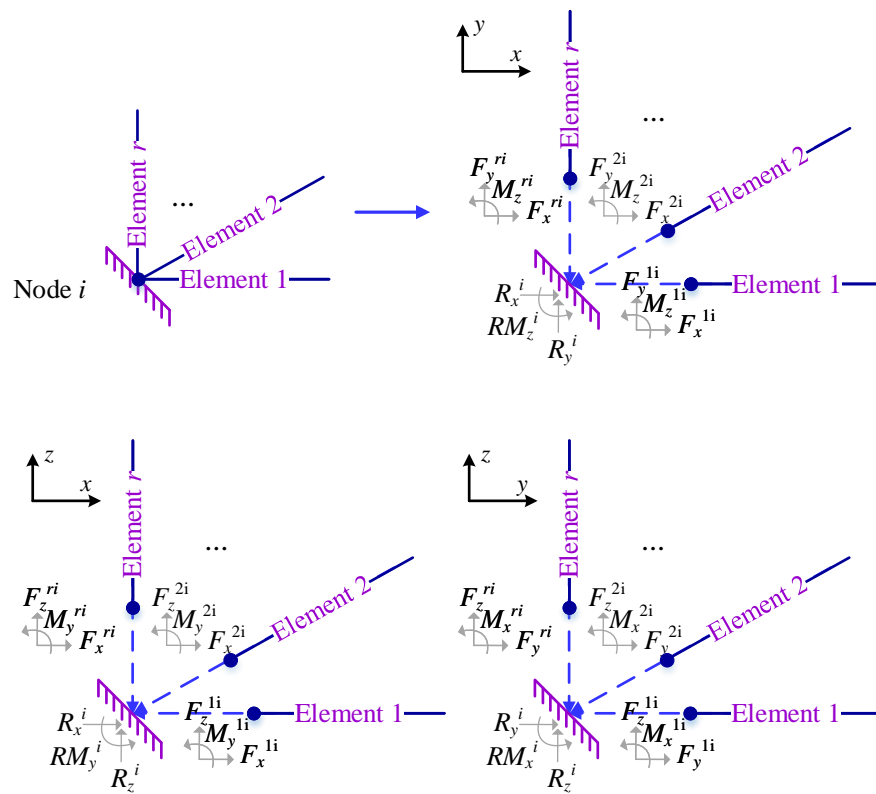


Figure A. .3 Equilibrium at a node  $i$

## Acknowledgement

The present research was performed under the support of the MEXT scholarship of Japan.

## 480 References

### References

- [1] P. G. Bakir, E. Reynders, G. De Roeck, Sensitivity-based finite element model updating using constrained optimization with a trust region algorithm, *Journal of Sound and Vibration* 305 (1-2) (2007) 211–225.
- 485 [2] Z. Zheng, Z. Lu, W. Chen, J. Liu, Structural damage identification based on power spectral density sensitivity analysis of dynamic responses, *Computers & Structures* 146 (2015) 176–184.
- [3] Z. Lu, S. Law, Features of dynamic response sensitivity and its application in damage detection, *Journal of Sound and Vibration* 303 (1-2) (2007) 305–  
490 329.
- [4] G. Liu, S. Chen, A novel technique for inverse identification of distributed stiffness factor in structures, *Journal of Sound and Vibration* 254 (5) (2002) 823–835.
- [5] O. Begambre, J. E. Laier, A hybrid particle swarm optimization–simplex  
495 algorithm (PSOS) for structural damage identification, *Advances in Engineering Software* 40 (9) (2009) 883–891.
- [6] A. Hera, Z. Hou, Application of wavelet approach for asce structural health monitoring benchmark studies, *Journal of Engineering Mechanics* 130 (1) (2004) 96–104.
- 500 [7] N. Roveri, A. Carcaterra, Damage detection in structures under traveling loads by hilbert–huang transform, *Mechanical Systems and Signal Processing* 28 (2012) 128–144.

- [8] B. Jaishi, W.-X. Ren, Damage detection by finite element model updating using modal flexibility residual, *Journal of Sound and Vibration* 290 (1-2) (2006) 369–387.
- [9] Z.-R. Lu, L. Wang, An enhanced response sensitivity approach for structural damage identification: convergence and performance, *International journal for numerical methods in engineering* 111 (13) (2017) 1231–1251.
- [10] J. Cunha, S. Cogan, C. Berthod, Application of genetic algorithms for the identification of elastic constants of composite materials from dynamic tests, *International Journal for Numerical Methods in Engineering* 45 (7) (1999) 891–900.
- [11] G. Liu, S. Chen, Flaw detection in sandwich plates based on time-harmonic response using genetic algorithm, *Computer Methods in Applied Mechanics and Engineering* 190 (42) (2001) 5505–5514.
- [12] H.-P. Chen, T. S. Maung, Regularised finite element model updating using measured incomplete modal data, *Journal of Sound and Vibration* 333 (21) (2014) 5566–5582.
- [13] M. Kaouk, D. C. Zimmerman, Structural damage assessment using a generalized minimum rank perturbation theory, *AIAA Journal* 32 (4) (1994) 836–842.
- [14] I. Ojalvo, D. Pilon, Diagnostics for geometrically locating structural math model errors from modal test data, in: *29th Structures, Structural Dynamics and Materials Conference*, 1988, p. 2358.
- [15] J. Guo, I. Takewaki, Minimum constitutive relation error based static identification of beams using force method, *Journal of Physics: Conference Series* 842 (1) (2017) 012026.
- [16] P. Feissel, O. Allix, Modified constitutive relation error identification strategy for transient dynamics with corrupted data: The elastic case, *Computer Methods in Applied Mechanics and Engineering* 196 (13) (2007) 1968–1983.

- [17] B. Blaysat, E. Florentin, G. Lubineau, A. Moussawi, A dissipation gap method for full-field measurement-based identification of elasto-plastic material parameters, *International Journal for Numerical Methods in Engineering* 91 (7) (2012) 685–704.
- 535 [18] M. Bonnet, A. Constantinescu, Inverse problems in elasticity, *Inverse Problems* 21 (2) (2005) R1.
- [19] B. Banerjee, T. F. Walsh, W. Aquino, M. Bonnet, Large scale parameter estimation problems in frequency-domain elastodynamics using an error in constitutive equation functional, *Computer Methods in Applied Mechanics and Engineering* 253 (2013) 60–72.
- 540 [20] B. Titurus, M. Friswell, Regularization in model updating, *International Journal for Numerical Methods in Engineering* 75 (4) (2008) 440–478.
- [21] C. Zhang, J.-Z. Huang, G.-Q. Song, L. Chen, Structural damage identification by extended kalman filter with  $\ell_1$ -norm regularization scheme, *Structural Control and Health Monitoring* 24 (11).
- 545 [22] E. M. Hernandez, Identification of isolated structural damage from incomplete spectrum information using  $\ell_1$ -norm minimization, *Mechanical Systems and Signal Processing* 46 (1) (2014) 59–69.
- [23] Y. Wang, H. Hao, Damage identification scheme based on compressive sensing, *Journal of Computing in Civil Engineering-ASCE* 29 (2) (2013) 04014037.
- 550 [24] V. A. Morozov, *Methods for solving incorrectly posed problems*, Springer Science & Business Media, 2012.
- [25] G. H. Golub, M. Heath, G. Wahba, Generalized cross-validation as a method for choosing a good ridge parameter, *Technometrics* 21 (2) (1979) 215–223.
- 555

- [26] P. C. Hansen, Analysis of discrete ill-posed problems by means of the l-curve, *SIAM review* 34 (4) (1992) 561–580.
- [27] D. Mascareñas, A. Cattaneo, J. Theiler, C. Farrar, Compressed sensing techniques for detecting damage in structures, *Structural Health Monitoring* 12 (4) (2013) 325–338.
- [28] Y. Yang, S. Nagarajaiah, Structural damage identification via a combination of blind feature extraction and sparse representation classification, *Mechanical Systems and Signal Processing* 45 (1) (2014) 1–23.
- [29] R. Hou, Y. Xia, Y. Bao, X. Zhou, Selection of regularization parameter for l1-regularized damage detection, *Journal of Sound and Vibration* 423 (2018) 141–160.
- [30] D.-H. Lee, W.-S. Hwang, Parametric optimization of complex systems using a multi-domain FRF-based substructuring method, *Computers & structures* 81 (22-23) (2003) 2249–2257.
- [31] F. Vestroni, D. Capecchi, Damage detection in beam structures based on frequency measurements, *Journal of Engineering Mechanics* 126 (7) (2000) 761–768.
- [32] A. Esfandiari, F. Bakhtiari-Nejad, A. Rahai, M. Sanayei, Structural model updating using frequency response function and quasi-linear sensitivity equation, *Journal of Sound and Vibration* 326 (3) (2009) 557–573.
- [33] P. Ladeveze, D. Leguillon, Error estimate procedure in the finite element method and applications, *SIAM Journal on Numerical Analysis* 20 (3) (1983) 485–509.
- [34] D. Barthe, A. Deraemaeker, P. Ladevèze, S. Le Loch, Validation and updating of industrial models based on the constitutive relation error, *AIAA journal* 42 (7).

- [35] A. Beck, On the convergence of alternating minimization for convex programming with applications to iteratively reweighted least squares and decomposition schemes, *SIAM Journal on Optimization* 25 (1) (2015) 185–209.
- [36] E. J. Candes, M. B. Wakin, S. P. Boyd, Enhancing sparsity by reweighted  $\ell_1$  minimization, *Journal of Fourier Analysis and Applications* 14 (5) (2008) 877–905.
- [37] M. Schmidt, Least squares optimization with  $L_1$ -norm regularization, CS542B Project Report (2005) 14–18.
- [38] M. Y. Park, T. Hastie,  $L_1$ -regularization path algorithm for generalized linear models, *Journal of the Royal Statistical Society: Series B (Statistical Methodology)* 69 (4) (2007) 659–677.
- [39] J. E. Mottershead, M. Link, M. I. Friswell, The sensitivity method in finite element model updating: a tutorial, *Mechanical systems and signal processing* 25 (7) (2011) 2275–2296.
- [40] Z.-R. Lu, J. Zhou, L. Wang, On choice and effect of weight matrix for response sensitivity-based damage identification with measurement and model errors, *Mechanical Systems and Signal Processing* 114 (2019) 1–24.
- [41] J. A. Dos Santos, C. M. Soares, C. M. Soares, N. Maia, Structural damage identification in laminated structures using FRF data, *Composite Structures* 67 (2) (2005) 239–249.
- [42] J. Friedman, T. Hastie, R. Tibshirani, The elements of statistical learning, Vol. 1, Springer series in statistics New York, 2001.